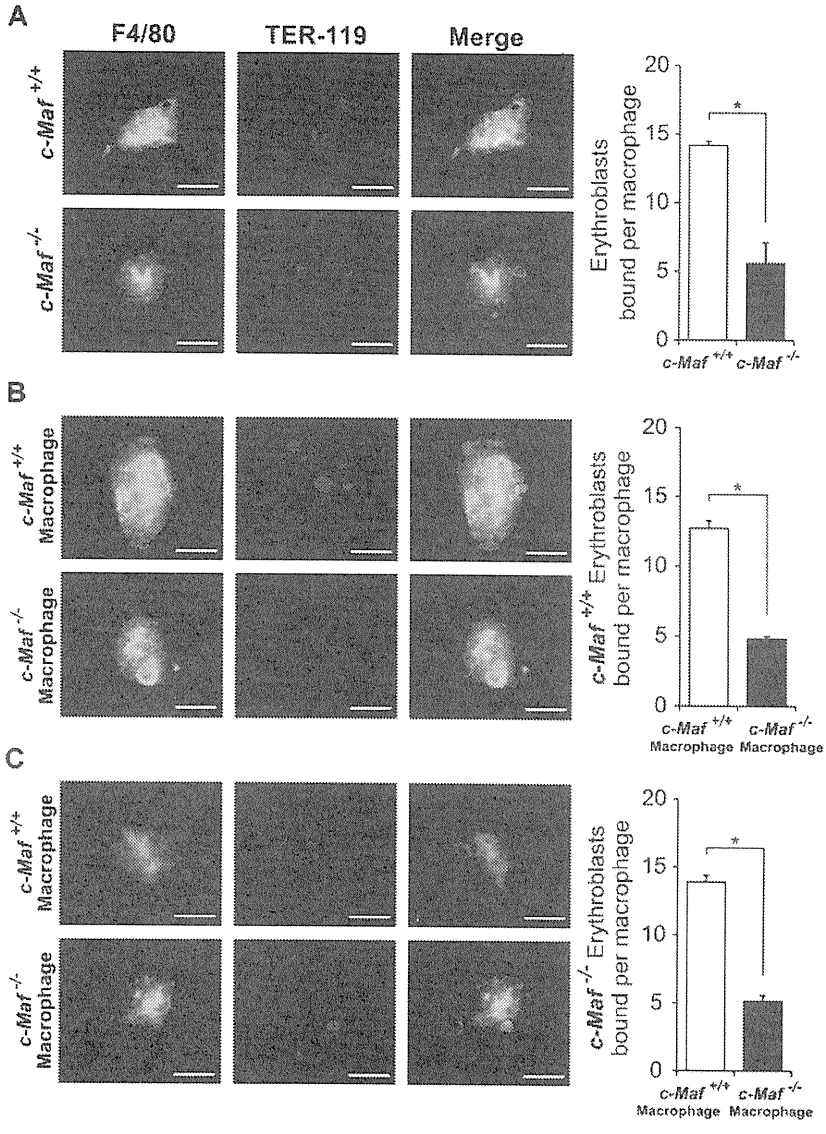

Figure 4. Absence of c-Maf impairs the formation of erythroblastic islands in the fetal liver. (A) Native erythroblastic islands isolated from *c-Maf*$^{+/+}$ and *c-Maf*$^{-/-}$ fetal liver were immunostained with F4/80 (green) and TER-119 (red) Abs as described in "Methods." F4/80 is used as a macrophage-specific marker, and TER-119 is used as a marker for erythroblasts. The number of erythroblasts surrounding each macrophage was significantly reduced in *c-Maf*$^{-/-}$ fetal liver. (B) Erythroblastic islands reconstituted with *c-Maf*$^{+/+}$ erythroblasts were immunostained. The number of *c-Maf*$^{+/+}$ erythroblasts surrounding each *c-Maf*$^{+/+}$ or *c-Maf*$^{-/-}$ macrophage is shown. *c-Maf*$^{+/+}$ erythroblasts surrounding *c-Maf*$^{-/-}$ macrophages were significantly reduced compared with those seen for *c-Maf*$^{+/+}$ macrophages. (C) Erythroblastic islands reconstituted with *c-Maf*$^{-/-}$ erythroblasts were immunostained. The number of *c-Maf*$^{-/-}$ erythroblasts surrounding each *c-Maf*$^{+/+}$ or *c-Maf*$^{-/-}$ macrophage is shown. *c-Maf*$^{-/-}$ erythroblasts surrounding *c-Maf*$^{-/-}$ macrophage were significantly reduced compared with those seen for *c-Maf*$^{+/+}$ macrophages. Although *c-Maf*$^{-/-}$ erythroblasts can form reconstituted erythroblastic islands with *c-Maf*$^{+/+}$ macrophages, *c-Maf*$^{-/-}$ macrophages showed impaired formation of reconstituted erythroblastic islands with *c-Maf*$^{+/+}$ erythroblasts. Images were acquired by a Biorevo BZ microscope (Plan Apo 20×0.75 DIC N2) at room temperature and processed with the Adobe Photoshop CS4 software. The scale bar represents 20 μm; n = 4~6 embryos per group. For each combination, ≥ 20 macrophages per embryo were analyzed. *$P < .05$. Data are presented as mean ± SEM.

number of CFU-E–, BFU-E–, and CFU-GEMM–derived colonies per fetal liver (Figure 3E). In addition, CFU-E colonies were indistinguishable in structure and size (supplemental Figure 4A-B). Moreover, erythroid cells derived from *c-Maf*$^{-/-}$ CFU-Es exhibited a similar structure, and enucleated red blood cells were also similar to those from *c-Maf*$^{+/+}$ control CFU-Es in cytospin slides stained with May-Grünwald-Giemsa (supplemental Figure 4C). Taken together, these results suggest that *c-Maf*$^{-/-}$ erythroid cells are still capable of developing into mature cells in vitro, in contrast to the result of flow cytometric analysis with the use of fetal liver cells (Figures 3A-C; supplemental Figure 2A-B), which reflects the in vivo condition. Therefore, the impaired definitive erythropoiesis in the *c-Maf*$^{-/-}$ embryos is more likely because of a non–cell-autonomous effect of c-Maf deficiency.

Absence of c-Maf causes impaired erythroblastic island formation in the fetal liver

c-Maf is abundantly expressed in fetal liver macrophages, although it is largely missing from the erythroid cells in fetal liver. Therefore, we initially surmised that c-Maf deficiency in fetal liver macrophages disturbed the erythroblastic islands.[3] To address this hypothesis, we attempted to examine whether *c-Maf*$^{-/-}$ macrophages failed to maintain the erythroblastic islands. For this purpose, we isolated the erythroblastic island from *c-Maf*$^{+/+}$ and *c-Maf*$^{-/-}$ fetal livers and counted the number of erythroblasts associated with each single central macrophage according to a previously described method.[31]

Interestingly, although > 10 TER-119^{+} erythroblasts were adhered to a F4/80^{+} macrophage in *c-Maf*$^{+/+}$ fetal livers, c-Maf–deficient central macrophages seemed to harbor far fewer erythroblasts (Figure 4). As shown in Figure 4A, the number of erythroblasts attached to a single central macrophage was significantly reduced in *c-Maf*$^{-/-}$ erythroblastic islands (14.2 ± 0.3 and 5.6 ± 1.5 erythroblasts per macrophage for *c-Maf*$^{+/+}$ and *c-Maf*$^{-/-}$, respectively). This result clearly indicates that erythroblastic islands are impaired in the *c-Maf*$^{-/-}$ fetal livers.

Next, to address whether c-Maf deficiency in macrophages was specifically responsible for the impairment of erythroblastic islands, a series of reconstitution experiments was performed. After attaching native erythroblastic islands either from *c-Maf*$^{+/+}$ or *c-Maf*$^{-/-}$ fetal livers on a glass coverslip, the adherent erythroblasts in the islands were stripped from the macrophages. Next, the

Table 2. Expression of genes comprising the macrophage signature

Symbol	Official full name	*c-Maf*$^{+/+}$ signal	*c-Maf*$^{-/-}$ signal	Fold
VCAM-1	Vascular cell adhesion molecule 1	8.3	1.6	0.19
Mrc1	Mannose receptor, C type 1	19.8	5.7	0.29
Csf1r	Colony stimulating factor 1 receptor	45	16.8	0.37
Sell	Selectin, lymphocyte	26.7	10	0.37
Lamp2	Lysosomal-associated membrane protein 2	8.9	3.3	0.37
Itgav	Integrin α V	1.2	0.5	0.41
Maea (EMP)	Macrophage erythroblast attacher	26.2	14.5	0.55
Emr1 (F4/80)	EGF-like module containing, mucin-like, hormone receptor-like sequence 1	71.4	48.1	0.67
Itgam (Mac-1)	Integrin α M	5.8	3.9	0.67
Cd163	CD163 antigen	0.6	0.4	0.67
Cd14	CD14 antigen	11.8	9.4	0.80
Fcgr1	Fc receptor, IgG, high-affinity I	15.7	17.6	1.12

Fetal liver macrophages were purified by flow cytometry from *c-Maf*$^{+/+}$ or *c-Maf*$^{-/-}$ fetal livers. The fold change in the gene expression was determined by dividing the signal obtained with *c-Maf*$^{-/-}$ fetal liver macrophage RNA by the signal obtained with *c-Maf*$^{+/+}$ RNA.

freshly isolated erythroblasts from *c-Maf*$^{+/+}$ or *c-Maf*$^{-/-}$ fetal livers were cocultured on the remaining adherent *c-Maf*$^{+/+}$ or *c-Maf*$^{-/-}$ fetal liver macrophages, respectively, so that *c-Maf*$^{+/+}$ erythroblasts were cocultured on *c-Maf*$^{-/-}$ central macrophages and vice versa. Surprisingly, *c-Maf*$^{-/-}$ macrophages failed to support erythroblastic islands with the inoculated wild-type

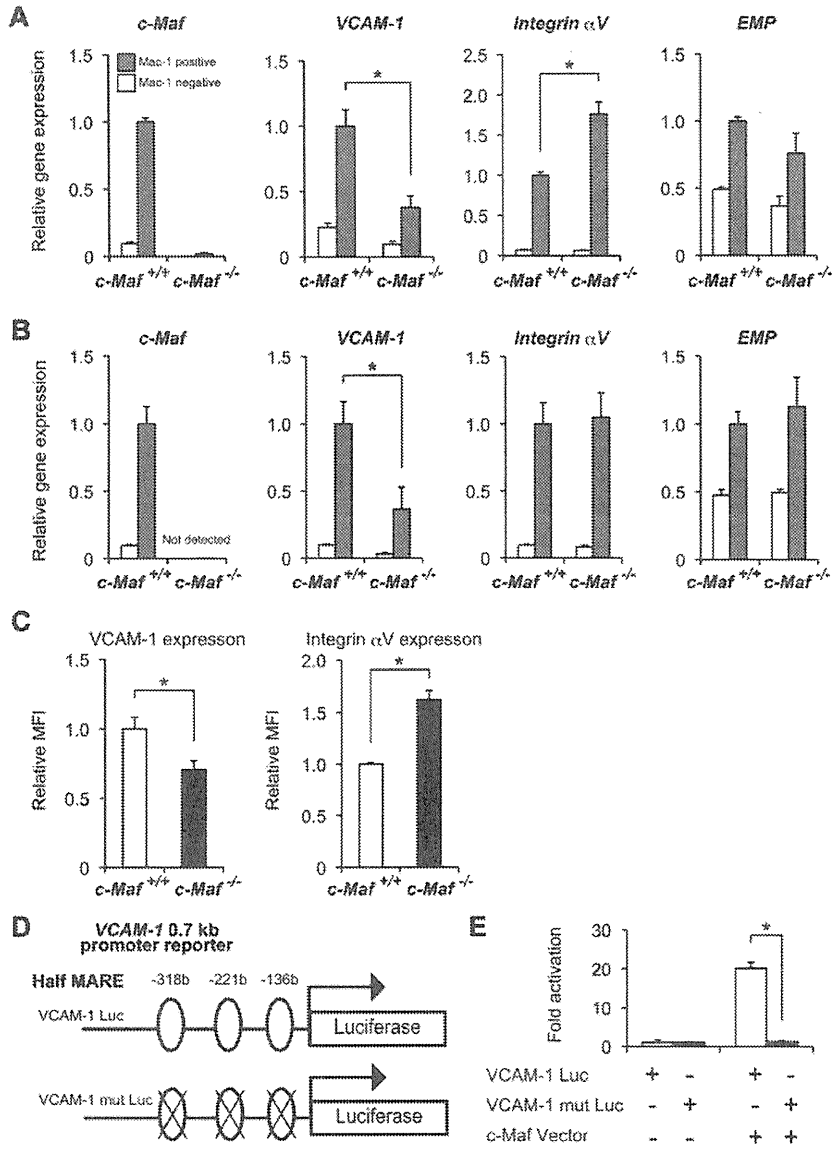

Figure 5. Decreased expression of VCAM-1 in *c-Maf*$^{-/-}$ fetal liver macrophage. mRNA expression profiles of erythroblast-macrophage adhesive interaction genes at E13.5 (A) and at E14.5 (B). Total RNA obtained from the Mac-1^{+} fraction (gray bar) and Mac-1^{-} fraction (open bar) of fetal liver cells was used for analyses. VCAM-1 expression was decreased in *c-Maf*$^{-/-}$ macrophages at E13.5 and E14.5; n = 7 per group; $^{*}P < .05$. The expression level of *c-Maf*$^{+/+}$ fetal liver Mac-1 fraction was set to 1.0. All of the data are presented as mean ± SEM (C) Relative mean fluorescent intensity (MFI) values of VCAM-1 and Integrin αV for the *c-Maf*$^{+/+}$ fetal liver Mac-1 fraction (normalized to MFI = 1) and the *c-Maf*$^{-/-}$ fetal liver Mac-1 fraction. E13.5 fetal liver cells were stained with FITC-conjugated anti–Mac-1 mAb, APC-conjugated anti–VCAM-1 mAb, and PE-conjugated anti-Integrin αV mAb. Bar graphs represent mean ratio ± SEM. Consistent with real-time RT-PCR analysis, significant differences in VCAM-1 and Integrin αV protein expression were observed; n = 8 per group; $^{*}P < .05$. (D) Schematic diagram of a luciferase reporter construct with the use of a VCAM-1 0.7-kb promoter (VCAM-1 Luc, top) ligated to a firefly luciferase cassette. Three putative half-MARE sites (5′ −318 bp, −221 bp, and −136 bp) are indicated. A luciferase assay was performed with a VCAM-1 Luc and that with mutations in half-MARE (VCAM-1 mut Luc, bottom) as reporters. (E) The pEFX3-FLAG-cMaf expression vector (c-Maf Vector) was cotransfected with the reporter plasmid into the macrophage cell line J774. The relative luciferase activity shown is derived from averages of 2 independent experiments (shown as mean ± SEM). The luciferase activity seen in J774 cells transfected with the reporter plasmid and with an empty vector was normalized to a value of 1 as the standard ($^{*}P < .05$).

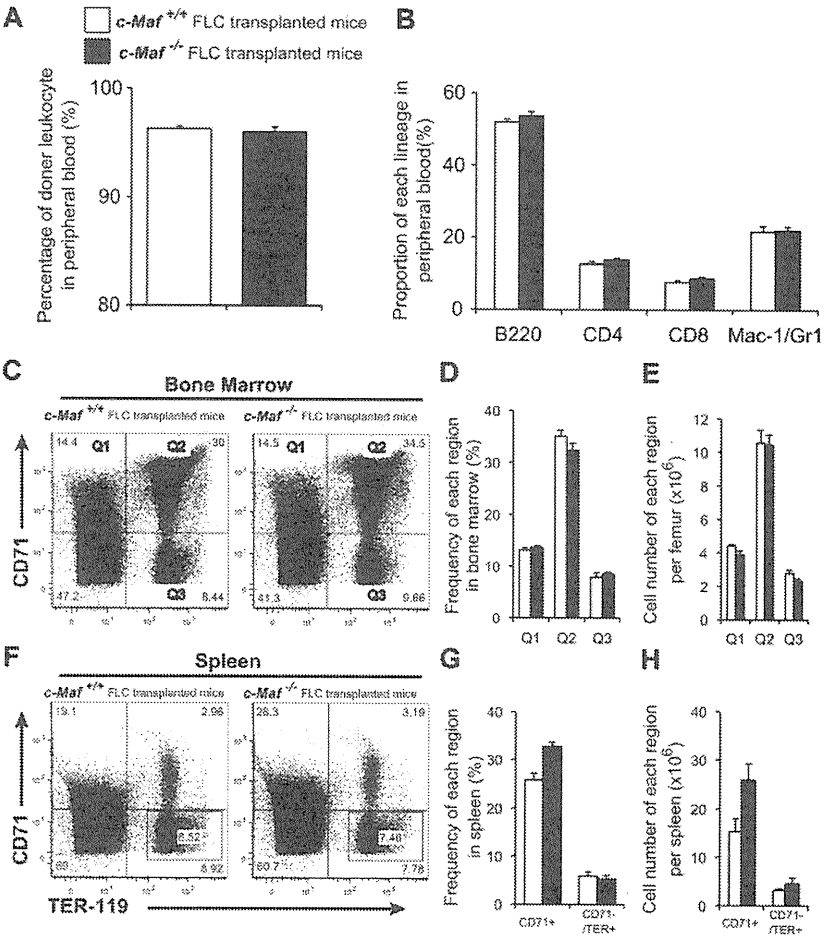

Figure 6. *c-Maf*$^{-/-}$ fetal liver cells can reconstitute adult hematopoiesis in lethally irradiated mice. (A) Eight to 10 weeks after transplantation, the donor leukocyte chimerism of the mice reconstituted with *c-Maf*$^{-/-}$ fetal liver cells was comparable to that of the mice reconstituted with *c-Maf*$^{+/+}$ fetal liver cells. The reconstitution efficiency was checked by flow cytometry with the use of the Ly5.1/Ly5.2 ratio of peripheral blood cells. Donor chimerism was determined to be as follows: (%Ly5.1$^+$/%Ly5.1$^+$ + %Ly5.2$^+$) × 100. (B) No significant difference was found in the proportion of each lineage in peripheral blood between *c-Maf*$^{+/+}$ fetal liver cells transplanted into mice and *c-Maf*$^{-/-}$ fetal liver cells transplanted into mice. (C) Flow cytometric analyses of the TER-119 and CD71 expression in total BM cells prepared from the femur of mice that received a transplant with *c-Maf*$^{+/+}$ fetal liver cells (left) or *c-Maf*$^{-/-}$ fetal liver cells (right). The gates of CD71$^+$/TER-119$^-$ (top left region: Q1), CD71$^+$/TER-119$^+$ (top right region: Q2), and CD71$^-$/TER-119$^+$ (bottom right region: Q3) in BM cells are defined as indicated. (D) Frequencies (%) of cells found in each region are shown. (E) Cell numbers of each region per femur are shown. (F) Flow cytometric analyses of the TER-119 and CD71 expression in total spleen cells prepared from mice that received a transplant with *c-Maf*$^{+/+}$ fetal liver cells (left) and *c-Maf*$^{-/-}$ fetal liver cells (right). The frequencies (%) of CD71$^+$ (top left and top right regions) and CD71$^-$/TER-119$^+$ (indicated squared gate in the bottom right region) cells in the spleen are indicated. (G) Frequencies (%) of each region are shown. (H) Cell numbers of each region per spleen are shown. Note that there are no significantly different frequencies or numbers of BM or spleen cells between mice that received a transplant with *c-Maf*$^{+/+}$ fetal liver cells versus with *c-Maf*$^{-/-}$ fetal liver cells. □ represents mice that received a transplant with *c-Maf*$^{+/+}$ fetal liver cells; ■, mice that received a transplant with *c-Maf*$^{-/-}$ fetal liver cells; n = 4 per group. FLC indicates, fetal liver cell.

erythroblasts (12.7 ± 0.5 erythroblasts per *c-Maf*$^{+/+}$ macrophage and 4.8 ± 0.2 erythroblasts per *c-Maf*$^{-/-}$ macrophage; Figure 4B). In contrast, *c-Maf*$^{-/-}$ erythroblasts were still capable of attaching to *c-Maf*$^{+/+}$ macrophages to the same extent as wild-type erythroblasts (13.9 ± 0.5 erythroblasts per *c-Maf*$^{+/+}$ macrophage and 5.1 ± 0.4 erythroblasts per *c-Maf*$^{-/-}$ macrophage; Figure 4C). These results show that the erythropoietic defects in *c-Maf*$^{-/-}$ embryos could be induced by an impaired hematopoietic microenvironment. Most probably, the suppressed functions of c-Maf–deficient central macrophages were responsible for the damaged erythroblastic islands.

Identification of target genes of c-Maf in fetal liver macrophages

To identify the molecular targets by which c-Maf regulates formation of erythroblastic islands in macrophages, we monitored the expression of cell adhesion molecules by microarray analysis. The expression of several important adhesion molecules was decreased in *c-Maf*$^{-/-}$ macrophages (Table 2). Expression of *VCAM-1* was suppressed the furthest in these molecules. To confirm the results from microarray analysis, we performed quantitative RT-PCR analyses, examining expression levels of *VCAM-1*, *Integrin* α*V*, and *EMP*. These are essential for erythroblastic island formation and maintenance and are thus designated as erythroblast-macrophage adhesive molecules.[3] The Mac-1$^+$ cells from either E13.5 or E14.5 fetal liver were sorted and analyzed to determine the mRNA abundance of these genes by real-time RT-PCR analysis. Of note, we observed an ~ 2.5-fold reduction in the *VCAM-1* mRNA expression level in the Mac-1$^+$ fraction from *c-Maf*$^{-/-}$ fetal liver, compared with the *c-Maf*$^{+/+}$ control at E13.5 and E14.5 (Figure 5A-B). However, *EMP* mRNA expression was not reduced in *c-Maf*$^{-/-}$ compared with *c-Maf*$^{+/+}$ (Figure 5A-B). In addition, expression of *Integrin* α*V* at E13.5 in *c-Maf*$^{-/-}$ was significantly up-regulated. Consistent with this observation, flow cytometric analysis of the fetal liver cells at E13.5 also verified a significant reduction of VCAM-1 protein expression in the *c-Maf*$^{-/-}$ fetal liver Mac-1$^+$ cells compared with the *c-Maf*$^{+/+}$ fetal liver Mac-1$^+$ cells, and protein expression of Integrin αV in the *c-Maf*$^{-/-}$ fetal liver Mac-1$^+$ cells was higher than that in *c-Maf*$^{+/+}$ (Figure 5C).

Given the significant suppression of VCAM-1 expression in *c-Maf*$^{-/-}$ fetal liver macrophages, we next addressed whether c-Maf could activate the *VCAM-1* gene promoter. To this end, a luciferase reporter assay in the J774 macrophage cell line was performed with a plasmid containing the 0.7-kb *VCAM-1* promoter region (VCAM-1 Luc) as a reporter (Figure 5D). The luciferase activity was significantly increased when the reporter plasmid was cotransfected with an expression plasmid for c-Maf. In contrast, when putative half-MARE sequences were mutated (VCAM-1 mut Luc), activation of the reporter was blunted (Figure 5E). These results indicate that c-Maf regulates the expression of *VCAM-1* by binding the putative half-MARE sites in its promoter region.

Table 3. Blood cell counts 6-12 weeks after fetal liver cell transplantation in mice

Genotype of transplanted FLC	*c-Maf*$^{+/+}$	*c-Maf*$^{-/-}$
WBC count, /μL	14 100 ± 1500	13 500 ± 1400
RBC count, ×10^4/μL	967 ± 10.0	949 ± 11.0
Hb level, g/dL	14.1 ± 0.2	13.9 ± 0.2
HCT, %	47.1 ± 0.7	46.8 ± 0.7
MCV, fL	48.7 ± 0.5	49.3 ± 0.4
MCH, pg	14.6 ± 0.2	14.6 ± 0.1
PLT count, ×10^4/μL	102.6 ± 5.8	92.3 ± 4.6

Values shown are the mean ± SEM for 20 mice per genotype. Mice with ≥ 90% donor leukocyte chimerism were used for analysis. *P* values were all NS.

FLC indicates fetal liver cell; WBC, white blood cell; RBC, red blood cell; Hb, hemoglobin; HCT, hematocrit; MCV, mean corpuscular volume; MCH, mean corpuscular hemoglobin; and PLT, platelet.

c-Maf–deficient fetal liver cells are capable of reconstituting the hematopoietic system of adult mice

To determine whether *c-Maf*$^{-/-}$ embryos still retain functional hematopoietic stem cells, we tested the ability of *c-Maf*–deficient fetal liver cells to reconstitute the hematopoietic system of lethally irradiated recipient mice. Fetal liver cells collected from E14.5 *c-Maf*$^{+/+}$ or *c-Maf*$^{-/-}$ embryos were injected into lethally irradiated recipient mice. All recipients receiving both *c-Maf*$^{+/+}$ and *c-Maf*$^{-/-}$ fetal liver cells survived and remained healthy for ≥ 6 months after transplantation. The donor-derived leukocyte chimerism in the mice reconstituted with *c-Maf*$^{-/-}$ fetal liver cells was comparable with that of the recipient mice with control fetal liver cells (Figure 6A). Moreover, there were no significant differences in hematocrit or proportion (%) of B220$^+$, CD4$^+$, CD8$^+$, or Mac-1$^+$/Gr1$^+$ cells between the recipients receiving *c-Maf*$^{+/+}$ or *c-Maf*$^{-/-}$ fetal liver cells (Table 3; Figure 6B).

Next, we attempted to examine whether erythroblast differentiation in the BM and spleen was perturbed. The absolute number of BM cells (19.9 ± 1.69 and 18.3 ± 1.56 × 10^6 cells/femur for *c-Maf*$^{+/+}$ and *c-Maf*$^{-/-}$ fetal liver cells transplanted into mice, respectively) as well as the spleen weight (68.4 ± 3.28 and 73.8 ± 5.44 mg for *c-Maf*$^{+/+}$ and *c-Maf*$^{-/-}$ fetal liver cells transplanted into mice, respectively) were comparable between mice that received a transplant with *c-Maf*$^{+/+}$ and *c-Maf*$^{-/-}$ fetal liver cells. Each stage of the erythroblasts was prospectively separated by a flow cytometric protocol that used TER-119 and CD71 Abs. The frequencies and cell numbers of each region in the recipient BM receiving *c-Maf*$^{-/-}$ fetal liver cells were comparable to those in the recipient with *c-Maf*$^{+/+}$ fetal liver cells (Figure 6C-E). Similar results were also observed with spleen cells (Figure 6F-H). Applying another method that TER-119 and CD44 Abs,[30] we assessed erythropoiesis in the BM of the mice that received a transplant. The differentiation status was found to be comparable between the recipients with *c-Maf*$^{+/+}$ and *c-Maf*$^{-/-}$ fetal liver cells (supplemental Figure 5A-C). Overall, these results indicate that *c-Maf*$^{-/-}$ hematopoietic cells are able to reconstitute the hematopoietic system in lethally irradiated mice and that they have the ability to produce adequate amounts of erythroid cells.

c-Maf deficiency does not impair erythropoiesis during PHZ-induced anemia

To assess the role of c-Maf in adult hematopoiesis further, we analyzed BM macrophages in a similar manner as that used to analyze fetal liver cells. The donor-derived BM leukocyte and BM macrophage chimerisms in the mice reconstituted with *c-Maf*$^{-/-}$ fetal liver cells were comparable with those of the recipient mice with control fetal liver cells (supplemental Figure 6). To determine whether *VCAM-1* mRNA levels were decreased, Mac-1$^+$ cells from the BM of mice that received a transplant were sorted and analyzed for mRNA abundance of *Mac-1*, *c-Maf*, *VCAM-1*, and *Integrin αV* by real-time RT-PCR analysis. These experiments showed no differences in expression levels in mice that received a transplant with *c-Maf*$^{+/+}$ and *c-Maf*$^{-/-}$ fetal liver cells except for *c-Maf* (Figure 7A), in contrast to the results obtained with the use of fetal

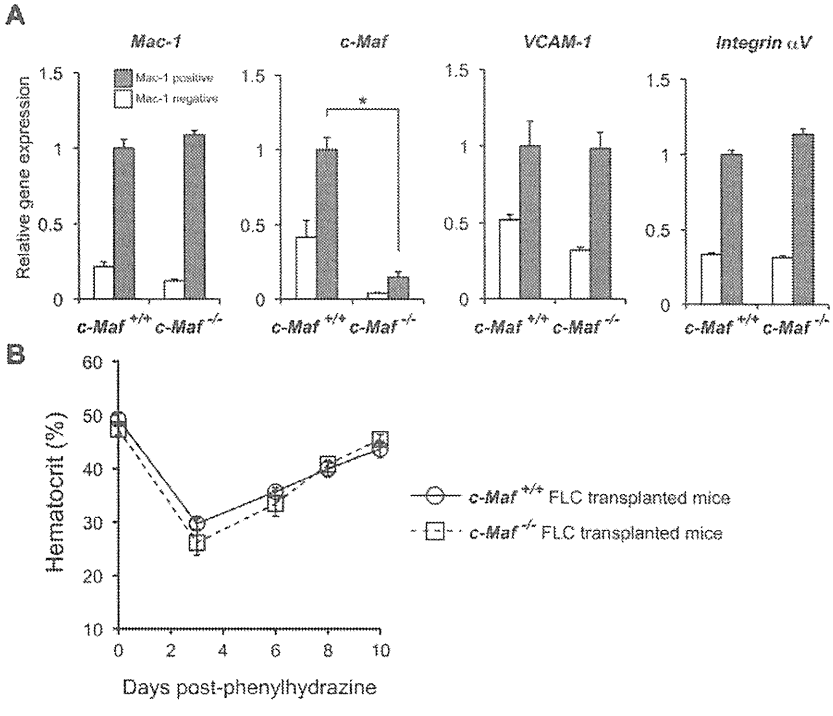

Figure 7. Responses of mice that received a transplant with *c-Maf*$^{-/-}$ fetal liver cells to induce anemia. (A) Comparisons of mRNA expression of *Mac-1*, *c-Maf*, *VCAM-1*, and *Integrin αV* are shown. Total RNA obtained from the Mac-1$^+$ positive fraction (gray bar) and the Mac-1$^-$ fraction (open bar) of BM cells was used for analyses. Note that *VCAM-1* mRNA expression of the Mac-1$^+$ fraction in mice that received a transplant with *c-Maf*$^{-/-}$ fetal liver cells is comparable with that of control mice that received a transplant with *c-Maf*$^{+/+}$ fetal liver cells; n = 5 per group; FLC indicates fetal liver cell; Expression of the *c-Maf*$^{+/+}$ BM Mac-1 fraction was set to 1.0. All of the data are presented as mean ± SEM. (B) Mice with a baseline hematocrit of ≥ 35% were used. Four mice that received a transplant with *c-Maf*$^{+/+}$ fetal liver cells (open circle with solid line) and 4 mice that received a transplant with *c-Maf*$^{-/-}$ fetal liver cells (open square with dashed line) were injected with phenylhydrazine on days 0, 1, and 3. Hematocrit levels were assessed on days 0, 3, 6, 8, and 10. Data are mean ± SEM.

liver cells. To reconfirm these results with a functional assay, mice were challenged with PHZ, and their hematocrits were monitored for the next 10 days (Figure 7B). The hematocrits of mice from both groups were comparable during this period. These results indicate that c-Maf deficiency does not impair stress erythropoiesis during PHZ-induced anemia in adult mice.

Discussion

Macrophages are important for hematopoiesis because they engulf nuclei of erythroblasts in erythroblastic islands, where the macrophages are surrounded by erythroblasts in the fetal liver, BM, and spleen.[3] In the present study, we demonstrated that c-Maf is crucial for the function of macrophages in erythropoiesis.

Our study clearly shows that disruption of c-Maf causes impaired erythroblastic island formation because of dysfunction of fetal liver macrophages. In a methylcellulose culture system, *c-Maf*$^{-/-}$ hematopoietic stem/progenitor cells in fetal liver have a normal potential to differentiate into different lineages, and they can reconstitute the hematopoietic system of lethally irradiated mice. Because c-Maf is specifically expressed in macrophages within the fetal liver, it has been thought that c-Maf does not regulate fetal liver erythropoiesis through a function of erythroblasts, but rather that it performs an adhesive function of macrophages. There are several reports of genes that are related to the formation and maintenance of erythroblastic islands, based on the knockout mice technique. Retinoblastoma-deficient mice were analyzed for macrophage differentiation, and erythroblastic island formation was reported to be impaired in these mice.[31] The fetal livers of *Dnase2a*$^{-/-}$ mice contain many macrophages that carry undigested DNA, and IFN-β mRNA was expressed by the resident macrophages in the *Dnase2a*$^{-/-}$ fetal liver.[37,38] In *c-Maf*$^{-/-}$ fetal livers, retinoblastoma was comparably expressed in *c-Maf*$^{+/+}$ and *c-Maf*$^{-/-}$ macrophages; therefore, the existence of impaired erythroblastic islands in *c-Maf*$^{-/-}$ mice is not related to retinoblastoma (supplemental Figure 7). In addition, we could not detect the abnormal foci that are found in *Dnase2a*$^{-/-}$ fetal livers or the expression of *IFN*-β mRNA (data not shown). Thus, retinoblastoma or DNase II do not cause the impaired erythroblastic islands of *c-Maf*$^{-/-}$ embryos.

To identify the target genes of c-Maf in fetal liver macrophages, we performed microarray analysis and found that VCAM-1 was one of these target genes. VCAM-1 is an adhesion molecule expressed on macrophages of erythroblastic islands. Previous studies have shown that maintenance of erythroblastic islands was impaired by an anti–VCAM-1 Ab.[8,39] As shown in Figure 5, mRNA and cell surface protein expression of VCAM-1 was decreased in *c-Maf*$^{-/-}$ fetal liver macrophages. This suggests that decreased expression of *VCAM-1* may be at least in part responsible for impaired erythroblastic island maintenance in *c-Maf*$^{-/-}$ fetal liver. The large Maf proteins are known to bind MAREs or the 5′ AT-rich half-MARE. In the *VCAM-1* promoter region, there are 3 half-MARE sites, so c-Maf may directly regulate *VCAM-1* expression in fetal liver macrophages. Recently, Kohyama et al[40] revealed that Spi-C controls the development of red pulp macrophages required for red blood cell recycling, and it regulates *VCAM-1* expression in red pulp macrophages. These earlier results and ours suggest that the regulation of *VCAM-1* expression by transcription factors strongly affects the function of tissue macrophages. In macrophages, c-Maf regulates the expression of cell surface molecules that are involved in macrophage function. In this analysis, expression of Integrin αV in *c-Maf*$^{-/-}$ macrophages was transiently up-regulated. It is difficult to identify the mechanism, but it seems probable there may be a compensation mechanism causing down-regulation of VCAM-1 in fetal macrophages.

We found that c-Maf is crucial for erythroblastic island maintenance in the embryonic stage. In a reconstitution assay that used fetal liver cells, *c-Maf*$^{-/-}$ hematopoietic cells reconstituted hematopoiesis in lethally irradiated mice, and the mice that received a transplant with *c-Maf*$^{-/-}$ fetal liver cells did not show anemia in the steady state (Table 3). To test the function of c-Maf in the adult stage further, we analyzed the mice that received a transplant by BM cell assay and by a PHZ stress test. Neither decreased expression level of *VCAM-1* mRNA nor impaired erythroid differentiation were observed. In addition, the response to the PHZ stress test was also comparable between the 2 groups. These results indicate that c-Maf might activate the VCAM-1 gene and affect erythroblastic island maintenance in a context-dependent manner. Such observations were reported previously. In *Palld*$^{-/-}$ fetal liver, erythroblastic island formation or integrity was impaired, but *Palld*$^{-/-}$ fetal liver cells could reconstitute the blood of lethally irradiated mice.[6] Thus, c-Maf and Palladin are important for erythroblastic islands in the embryonic stage, but their importance in the adult stage is still unconfirmed. However, a previous study found that ICAM-4 is critical for erythroblastic island formation in adult marrow,[41] but the role of ICAM-4 in the embryonic stage has been left for future study. Overall, previous studies and our results indicate that there might be different mechanisms or regulation processes or both between fetal liver and adult marrow/spleen erythroblastic island formation and maintenance. This suggests that macrophages in fetal liver and in the adult marrow/spleen might have different developmental origins. Further studies are needed to investigate this possibility.

Recent reports have indicated that definitive as well as primitive erythropoiesis are related to erythroblastic islands.[39] Kingsley et al[42] revealed that yolk sac-derived primitive erythroblasts enucleate during gestation, and Isern et al[39] and Fraser et al[43] also have demonstrated, using transgenic mouse lines, that primitive erythroblasts enucleate within the fetal liver.[39,43] Our quantitative RT-PCR results suggested that definitive erythropoiesis is more involved in erythroblastic islands than is primitive erythropoiesis in vivo (supplemental Figure 3). Therefore, this result indicates that definitive erythropoiesis in fetal liver is predominantly impaired in *c-Maf*$^{-/-}$ embryos, whereas primitive erythropoiesis is maintained in *c-Maf*$^{-/-}$ embryos.

Our study showed that *c-Maf*$^{-/-}$ mice were embryonic lethal on the C57BL/6 background and that *c-Maf*$^{-/-}$ macrophages might be responsible for this. Previous reports from our laboratory and from others indicated that *c-Maf*$^{-/-}$ mice were lethal around birth on the C57BL/6J × 129/SV background, but some mice on the BALB/c background live to adulthood.[14,44,45] It is known that cytokine production in T-helper cells differs between C57BL/6 and BALB/c backgrounds. Recently Mills at al[46] reported that cytokine production in macrophages differed according to the backgrounds of the mice. On a C57BL/6 background, inflammatory cytokine production is more dominant than on a BALB/c background. It is well known that apoptotic cells are recognized by macrophages and induce the production of proinflammatory cytokines.[47] Increased amounts of apoptotic cells were observed in *c-Maf*$^{-/-}$ fetal liver, suggesting that inflammatory cytokine production might be triggered in *c-Maf*$^{-/-}$ fetal liver. Therefore, our *c-Maf*$^{-/-}$ mice were lethal at an earlier gestational date than indicated by previous reports. We found that *c-Maf*$^{-/-}$ fetal liver macrophages produced

more cytokines than *c-Maf*$^{+/+}$ fetal liver macrophages (supplemental Figure 7). Hence, it is tempting to speculate that increased numbers of apoptotic cells trigger the production of inflammatory cytokines that are reported to be responsible for anemia and embryonic lethality. This speculation supports the idea that the *c-Maf*$^{-/-}$ macrophages are responsible for anemia and lethality. This hypothesis may also explain the phenotype discrepancy between *c-Maf*$^{-/-}$ mice and *F4/80*$^{-/-}$ or *VCAM-1*$^{-/-}$ mice. Neither F4/80 knockout mice nor mice with a conditional ablation of VCAM-1 in blood cells are embryonic lethal.[48-50] In addition, c-Maf is a transcription factor, and it might regulate sets of target genes in fetal macrophages that might in turn be responsible for the observed anemia and lethality.

In summary, we have shown that the transcription factor c-Maf gene affects the hematopoietic microenvironment by playing a crucial role in regulating fetal liver macrophages.

Acknowledgments

The authors thank Dr Yamashita and Dr Ohneda for the *VCAM-1* promoter containing luciferase plasmid.

This work was supported by a Grant-in-Aid for Scientific Research (KAKENHI no. 21220009) from the Ministry of Education, Culture, Sports, Science and Technology of Japan (MEXT). This work was also supported by Grants from the Astellas Foundation for Research on Metabolic Disorders and the Uehara Memorial Foundation. M.K. is a recipient of a Japan Society for the Promotion of Science Research Fellowship for Young Scientists (21384).

Authorship

Contribution: M.K., K.H., M.H., M.N., T.O., H.S., and M.T.N.T. performed experiments; M.K., K.H., and M.H. analyzed results and made figures; M.K., K.H., M.H., and S.T. designed the research; M.K., M.H., and S.T. wrote the paper; K.U. performed microarray analysis; and T.K., H.N., S.C., and S.T. supervised the project.

Conflict-of-interest disclosure: The authors declare no competing financial interests.

Correspondence: Satoru Takahashi, Departments of Anatomy and Embryology, Institute of Basic Medical Science, University of Tsukuba, 1-1-1 Tennodai, Tsukuba, Ibaraki 305-8575, Japan; e-mail: satoruta@md.tsukuba.ac.jp.

References

1. Palis J. Ontogeny of erythropoiesis. *Curr Opin Hematol.* 2008;15(3):155-161.
2. Allen TD, Dexter TM. Ultrastructural aspects of erythropoietic differentiation in long-term bone marrow culture. *Differentiation.* 1982;21(2):86-94.
3. Chasis JA, Mohandas N. Erythroblastic islands: niches for erythropoiesis. *Blood.* 2008;112(3): 470-478.
4. Hanspal M, Hanspal JS. The association of erythroblasts with macrophages promotes erythroid proliferation and maturation: a 30-kD heparin-binding protein is involved in this contact. *Blood.* 1994;84(10):3494-3504.
5. Mohandas N, Prenant M. Three-dimensional model of bone marrow. *Blood.* 1978;51(4):633-643.
6. Liu X-S, Li X-H, Wang Y, et al. Disruption of palladin leads to defects in definitive erythropoiesis by interfering with erythroblastic island formation in mouse fetal liver. *Blood.* 2007;110(3):870-876.
7. Soni S, Bala S, Gwynn B, Sahr KE, Peters LL, Hanspal M. Absence of erythroblast macrophage protein (Emp) leads to failure of erythroblast nuclear extrusion. *J Biol Chem.* 2006;281(29): 20181-20189.
8. Sadahira Y, Yoshino T, Monobe Y. Very late activation antigen 4-vascular cell adhesion molecule 1 interaction is involved in the formation of erythroblastic islands. *J Exp Med.* 1995;181(1):411-415.
9. Nishizawa M, Kataoka K, Goto N, Fujiwara KT, Kawai S. v-maf, a viral oncogene that encodes a "leucine zipper" motif. *Proc Natl Acad Sci U S A.* 1989;86(20):7711-7715.
10. Kataoka K, Fujiwara KT, Noda M, Nishizawa M. MafB, a new Maf family transcription activator that can associate with Maf and Fos but not with Jun. *Mol Cell Biol.* 1994;14(11):7581-7591.
11. Kataoka K, Noda M, Nishizawa M. Maf nuclear oncoprotein recognizes sequences related to an AP-1 site and forms heterodimers with both Fos and Jun. *Mol Cell Biol.* 1994;14(1):700-712.
12. Yoshida T, Ohkumo T, Ishibashi S, Yasuda K. The 5′-AT-rich half-site of Maf recognition element: a functional target for bZIP transcription factor Maf. *Nucleic Acids Res.* 2005;33(11): 3465-3478.
13. Kajihara M, Kawauchi S, Kobayashi M, Ogino H, Takahashi S, Yasuda K. Isolation, characterization, and expression analysis of zebrafish large Mafs. *J Biochem.* 2001;129(1):139-146.
14. Kawauchi S, Takahashi S, Nakajima O, et al. Regulation of lens fiber cell differentiation by transcription factor c-Maf. *J Biol Chem.* 1999;274(27): 19254-19260.
15. Moriguchi T, Hamada M, Morito N, et al. MafB is essential for renal development and F4/80 expression in macrophages. *Mol Cell Biol.* 2006; 26(15):5715-5727.
16. Ogino H, Yasuda K. Induction of lens differentiation by activation of a bZIP transcription factor, L-Maf. *Science.* 1998;280(5360):115-118.
17. Sieweke MH, Tekotte H, Frampton J, Graf T. MafB is an interaction partner and repressor of Ets-1 that inhibits erythroid differentiation. *Cell.* 1996;85(1):49-60.
18. Swaroop A, Xu JZ, Pawar H, Jackson A, Skolnick C, Agarwal N. A conserved retina-specific gene encodes a basic motif/leucine zipper domain. *Proc Natl Acad Sci U S A.* 1992;89(1):266-270.
19. Zhang C, Moriguchi T, Kajihara M, et al. MafA is a key regulator of glucose-stimulated insulin secretion. *Mol Cell Biol.* 2005;25(12):4969-4976.
20. Eychene A, Rocques N, Pouponnot C. A new MAFia in cancer. *Nat Rev Cancer.* 2008;8(9):683-693.
21. Hurt EM, Wiestner A, Rosenwald A, et al. Overexpression of c-maf is a frequent oncogenic event in multiple myeloma that promotes proliferation and pathological interactions with bone marrow stroma. *Cancer Cell.* 2004;5(2):191-199.
22. Morito N, Yoh K, Fujioka Y, et al. Overexpression of c-Maf contributes to T-cell lymphoma in both mice and human. *Cancer Res.* 2006;66(2):812-819.
23. Murakami YI, Yatabe Y, Sakaguchi T, et al. c-Maf expression in angioimmunoblastic T-cell lymphoma. *Am J Surg Pathol.* 2007;31(11):1695-1702.
24. Bauquet AT, Jin H, Paterson AM, et al. The costimulatory molecule ICOS regulates the expression of c-Maf and IL-21 in the development of follicular T helper cells and TH-17 cells. *Nat Immunol.* 2009;10(2):167-175.
25. Ho IC, Hodge MR, Rooney JW, Glimcher LH. The proto-oncogene c-maf is responsible for tissue-specific expression of interleukin-4. *Cell.* 1996; 85(7):973-983.
26. Cao S, Liu J, Song L, Ma X. The protooncogene c-Maf is an essential transcription factor for IL-10 gene expression in macrophages. *J Immunol.* 2005;174(6):3484-3492.
27. Aziz A, Soucie E, Sarrazin S, Sieweke MH. MafB/c-Maf deficiency enables self-renewal of differentiated functional macrophages. *Science.* 2009; 326(5954):867-871.
28. Nakamura M, Hamada M, Hasegawa K, et al. c-Maf is essential for the F4/80 expression in macrophages in vivo. *Gene.* 2009;445(1-2):66-72.
29. Masuoka HC, Townes TM. Targeted disruption of the activating transcription factor 4 gene results in severe fetal anemia in mice. *Blood.* 2002;99(3): 736-745.
30. Chen K, Liu J, Heck S, Chasis JA, An X, Mohandas N. Resolving the distinct stages in erythroid differentiation based on dynamic changes in membrane protein expression during erythropoiesis. *Proc Natl Acad Sci U S A.* 2009;106(41): 17413-17418.
31. Iavarone A, King ER, Dai X-M, Leone G, Stanley ER, Lasorella A. Retinoblastoma promotes definitive erythropoiesis by repressing Id2 in fetal liver macrophages. *Nature.* 2004;432(7020):1040-1045.
32. Ema M, Mori D, Niwa H, et al. Kruppel-like factor 5 is essential for blastocyst development and the normal self-renewal of mouse ESCs. *Cell Stem Cell.* 2008;3(5):555-567.
33. Yamashita T, Ohneda O, Sakiyama A, Iwata F, Ohneda K, Fujii-Kuriyama Y. The microenvironment for erythropoiesis is regulated by HIF-2alpha through VCAM-1 in endothelial cells. *Blood.* 2008;112(4):1482-1492.
34. Angelillo-Scherrer A, Burnier L, Lambrechts D, et al. Role of Gas6 in erythropoiesis and anemia in mice. *J Clin Invest.* 2008;118(2):583-596.
35. Wu L, de Bruin A, Saavedra HI, et al. Extra-embryonic function of Rb is essential for embryonic development and viability. *Nature.* 2003; 421(6926):942-947.
36. Zhang J, Socolovsky M, Gross AW, Lodish HF.

Role of Ras signaling in erythroid differentiation of mouse fetal liver cells: functional analysis by a flow cytometry-based novel culture system. *Blood.* 2003;102(12):3938-3946.

37. Kawane K, Fukuyama H, Kondoh G, et al. Requirement of DNase II for definitive erythropoiesis in the mouse fetal liver. *Science.* 2001;292(5521):1546-1549.
38. Yoshida H, Okabe Y, Kawane K, Fukuyama H, Nagata S. Lethal anemia caused by interferon-beta produced in mouse embryos carrying undigested DNA. *Nat Immunol.* 2005;6(1):49-56.
39. Isern J, Fraser ST, He Z, Baron MH. The fetal liver is a niche for maturation of primitive erythroid cells. *Proc Natl Acad Sci U S A.* 2008;105(18):6662-6667.
40. Kohyama M, Ise W, Edelson BT, et al. Role for Spi-C in the development of red pulp macrophages and splenic iron homeostasis. *Nature.* 2009;457(7227):318-321.
41. Lee G, Lo A, Short SA, et al. Targeted gene deletion demonstrates that the cell adhesion molecule ICAM-4 is critical for erythroblastic island formation. *Blood.* 2006;108(6):2064-2071.
42. Kingsley PD, Malik J, Fantauzzo KA, Palis J. Yolk sac-derived primitive erythroblasts enucleate during mammalian embryogenesis. *Blood.* 2004;104(1):19-25.
43. Fraser ST, Isern J, Baron MH. Maturation and enucleation of primitive erythroblasts during mouse embryogenesis is accompanied by changes in cell-surface antigen expression. *Blood.* 2007;109(1):343-352.
44. Kim JI, Li T, Ho IC, Grusby MJ, Glimcher LH. Requirement for the c-Maf transcription factor in crystallin gene regulation and lens development. *Proc Natl Acad Sci U S A.* 1999;96(7):3781-3785.
45. Ring BZ, Cordes SP, Overbeek PA, Barsh GS. Regulation of mouse lens fiber cell development and differentiation by the Maf gene. *Development.* 2000;127(2):307-317.
46. Mills CD, Kincaid K, Alt JM, Heilman MJ, Hill AM. M-1/M-2 macrophages and the Th1/Th2 paradigm. *J Immunol.* 2000;164(12):6166-6173.
47. Nagata S, Hanayama R, Kawane K. Autoimmunity and the clearance of dead cells. *Cell.* 2010;140(5):619-630.
48. Lin HH, Faunce DE, Stacey M, et al. The macrophage F4/80 receptor is required for the induction of antigen-specific efferent regulatory T cells in peripheral tolerance. *J Exp Med.* 2005;201(10):1615-1625.
49. Schaller E, Macfarlane AJ, Rupec RA, Gordon S, McKnight AJ, Pfeffer K. Inactivation of the F4/80 glycoprotein in the mouse germ line. *Mol Cell Biol.* 2002;22(22):8035-8043.
50. Ulyanova T, Scott LM, Priestley GV, et al. VCAM-1 expression in adult hematopoietic and nonhematopoietic cells is controlled by tissue-inductive signals and reflects their developmental origin. *Blood.* 2005;106(1):86-94.

ARTICLE

doi:10.1038/nature10496

Frequent pathway mutations of splicing machinery in myelodysplasia

Kenichi Yoshida[1]*, Masashi Sanada[1]*, Yuichi Shiraishi[2]*, Daniel Nowak[3]*, Yasunobu Nagata[1]*, Ryo Yamamoto[4], Yusuke Sato[1], Aiko Sato-Otsubo[1], Ayana Kon[1], Masao Nagasaki[5], George Chalkidis[6], Yutaka Suzuki[7], Masashi Shiosaka[1], Ryoichiro Kawahata[1], Tomoyuki Yamaguchi[8], Makoto Otsu[4], Naoshi Obara[9], Mamiko Sakata-Yanagimoto[9], Ken Ishiyama[10], Hiraku Mori[11], Florian Nolte[3], Wolf-Karsten Hofmann[3], Shuichi Miyawaki[10], Sumio Sugano[7], Claudia Haferlach[12], H. Phillip Koeffler[13,14], Lee-Yung Shih[15], Torsten Haferlach[12], Shigeru Chiba[9], Hiromitsu Nakauchi[4,8], Satoru Miyano[2,6] & Seishi Ogawa[1]

Myelodysplastic syndromes and related disorders (myelodysplasia) are a heterogeneous group of myeloid neoplasms showing deregulated blood cell production with evidence of myeloid dysplasia and a predisposition to acute myeloid leukaemia, whose pathogenesis is only incompletely understood. Here we report whole-exome sequencing of 29 myelodysplasia specimens, which unexpectedly revealed novel pathway mutations involving multiple components of the RNA splicing machinery, including *U2AF35*, *ZRSR2*, *SRSF2* and *SF3B1*. In a large series analysis, these splicing pathway mutations were frequent (~45 to ~85%) in, and highly specific to, myeloid neoplasms showing features of myelodysplasia. Conspicuously, most of the mutations, which occurred in a mutually exclusive manner, affected genes involved in the 3′-splice site recognition during pre-mRNA processing, inducing abnormal RNA splicing and compromised haematopoiesis. Our results provide the first evidence indicating that genetic alterations of the major splicing components could be involved in human pathogenesis, also implicating a novel therapeutic possibility for myelodysplasia.

Myelodysplastic syndromes (MDS) and related disorders (myelodysplasia) comprise a group of myeloid neoplasms characterized by deregulated, dysplastic blood cell production and a predisposition to acute myeloid leukaemia (AML)[1]. Although the prevalence of MDS has not been determined precisely, more than 10,000 people are estimated to develop myelodysplasia annually in the United States[2]. Their indolent clinical course before leukaemic transformation and ineffective haematopoiesis with evidence of myeloid dysplasia indicate a pathogenesis distinct from that involved in *de novo* AML. Currently, a number of gene mutations and cytogenetic changes have been implicated in the pathogenesis of MDS, including mutations of *RAS*, *TP53* and *RUNX1*, and more recently *ASXL1*, *c-CBL*, *DNMT3A*, *IDH1/2*, *TET2* and *EZH2* (ref. 3). Nevertheless, mutations of this set of genes do not fully explain the pathogenesis of MDS because they are also commonly found in other myeloid malignancies and roughly 20% of MDS cases have no known genetic changes (ref. 4 and unpublished data). In particular, the genetic alterations responsible for the dysplastic phenotypes and ineffective haematopoiesis of myelodysplasia are poorly understood. Meanwhile, the recent development of massively parallel sequencing technologies has provided an expanded opportunity to discover genetic changes across the entire genomes or protein-coding sequences in human cancers at a single-nucleotide level[5–10], which could be successfully applied to the genetic analysis of myelodysplasia to obtain a better understanding of its pathogenesis.

Overview of genetic alterations

In this study, we performed whole-exome sequencing of paired tumour/control DNA from 29 patients with myelodysplasia (Supplementary Table 1). Although incapable of detecting non-coding mutations and gene rearrangements, the whole-exome approach is a well-established strategy for obtaining comprehensive registries of protein-coding mutations at low cost and high performance. With a mean coverage of 133.8, 80.4% of the target sequences were analysed at more than ×20 depth on average (Supplementary Fig. 1). All the candidates for somatic mutations ($N = 497$) generated through our data analysis pipeline were subjected to validation using Sanger sequencing (Supplementary Methods I and Supplementary Fig. 2). Finally, 268 non-synonymous somatic mutations were confirmed with an overall true positive rate of 53.9% (Supplementary Fig. 3), including 206 missense, 25 nonsense, and 10 splice site mutations, and 27 frameshift-causing insertions/deletions (indels) (Supplementary Fig. 4). The mutation rate of 9.2 (0–21) per sample was significantly lower than that in solid tumours (16.2–302)[7,11,12] and multiple myeloma (32.4)[6], but was comparable to that in AML (7.3–13)[13–15] and chronic lymphocytic leukaemia (11.5)[16]. Combined with the genomic copy number profile obtained by single nucleotide polymorphism (SNP) array karyotyping, this array of somatic mutations provided a landscape of myelodysplasia genomes (Supplementary Fig. 5)[17,18].

[1]Cancer Genomics Project, Graduate School of Medicine, The University of Tokyo, 7-3-1 Hongo, Bunkyo-ku, Tokyo 113-8655, Japan. [2]Laboratory of DNA Information Analysis, Human Genome Center, Institute of Medical Science, The University of Tokyo, 4-6-1 Shirokanedai, Minato-ku, Tokyo 108-8639, Japan. [3]Department of Hematology and Oncology, Medical Faculty Manheim of the University of Heidelberg, 1–3 Theodor-Kutzer-Ufer, Mannheim 68167, Germany. [4]Division of Stem Cell Therapy, Center for Stem Cell Biology and Regenerative Medicine, Institute of Medical Science, The University of Tokyo, 4-6-1 Shirokanedai, Minato-ku, Tokyo 108-8639, Japan. [5]Laboratory of Functional Genomics, Human Genome Center, Institute of Medical Science, The University of Tokyo, 4-6-1 Shirokanedai, Minato-ku, Tokyo 108-8639, Japan. [6]Laboratory of Sequence Data Analysis, Human Genome Center, Institute of Medical Science, The University of Tokyo, 4-6-1 Shirokanedai, Minato-ku, Tokyo 108-8639, Japan. [7]Division of Systems Biomedical Technology, Institute of Medical Science, The University of Tokyo, 4-6-1 Shirokanedai, Minato-ku, Tokyo 108-8639, Japan. [8]Nakauchi Stem Cell and Organ Regeneration Project, Exploratory Research for Advanced Technology, Japan Science and Technology Agency, 4-6-1 Shirokanedai, Minato-ku, Tokyo 108-8639, Japan. [9]Department of Hematology, Institute of Clinical Medicine, University of Tsukuba, 1-1-1 Tennodai, Tsukuba-shi, Ibaraki, 305-8571, Japan. [10]Division of Hematology, Tokyo Metropolitan Ohtsuka Hospital, 2-8-1 Minami-Ohtsuka, Toshima-ku, Tokyo 170-0005, Japan. [11]Division of Hematology, Internal Medicine, Showa University Fujigaoka Hospital, 1-30 Fujigaoka, Aoba-ku, Yokohama, Kanagawa 227-8501, Japan. [12]Munich Leukemia Laboratory, Max-Lebsche-Platz 31, Munich 81377, Germany. [13]Hematology/Oncology, Cedars-Sinai Medical Center, 8700 Beverly Blvd, Los Angeles, California 90048, USA. [14]National University of Singapore, Cancer Science Institute of Singapore, 28 Medical Drive, Singapore 117456, Singapore. [15]Division of Hematology-Oncology, Department of Internal Medicine, Chang Gung Memorial Hospital, Chang Gung University, 199 Tung Hwa North Rd, Taipei 105, Taiwan.
*These authors contributed equally to this work.

Novel gene targets in myelodysplasia

The list of the somatic mutations (Supplementary Table 2) included most of the known gene targets in myelodysplasia with similar mutation frequencies to those previously reported, indicating an acceptable sensitivity of the current study. The mutations of the known gene targets, however, accounted for only 12.3% of all detected mutations ($N = 33$), and the remaining 235 mutations involved previously unreported genes. Among these, recurrently mutated genes in multiple cases are candidate targets of particular interest, for which high mutation rates are expected in general populations. In fact, 8 of the 12 recurrently mutated genes were among the well-described gene targets in myelodysplasia (Supplementary Table 3). However, what immediately drew our attention were the recurrent mutations involving *U2AF35* (also known as *U2AF1*), *ZRSR2* and *SRSF2* (*SC35*), because they belong to the common pathway known as RNA splicing. Including an additional three genes mutated in single cases (*SF3A1*, *SF3B1* and *PRPF40B*), six components of the splicing machinery were mutated in 16 out of the 29 cases (55.2%) in a mutually exclusive manner (Fig. 1, Supplementary Fig. 6 and Supplementary Table 2).

Frequent mutations in splicing machinery

RNA splicing is accomplished by a well-ordered recruitment, rearrangement and/or disengagement of a set of small nuclear ribonucleoprotein (snRNP) complexes (U1, U2, and either U4/5/6 or U11/12), as well as many other protein components onto the pre-mRNAs. Notably, the mutated components of the spliceosome were all engaged in the initial steps of RNA splicing, except for PRPF40B, whose functions in RNA splicing are poorly defined. Making physical interactions with SF1 and a serine/arginine-rich (SR) protein, such as SRSF1 or SRSF2, the U2 auxiliary factor (U2AF) that consists of the U2AF65 (U2AF2)–U2AF35 heterodimer, is involved in the recognition of the 3′ splice site (3′SS) and its nearby polypyrimidine tract, which is thought to be required for the subsequent recruitment of the U2 snRNP, containing SF3A1 as well as SF3B1, to establish the splicing A complex (Fig. 1)[19]. ZRSR2 (or Urp), is another essential component of the splicing machinery. Showing a close structural similarity to U2AF35, ZRSR2 physically interacts with U2AF65, as well as SRSF1 and SRSF2, with a distinct function from its homologue, U2AF35 (ref. 20).

To confirm and extend the initial findings in the whole-exome sequencing, we studied mutations of the above six genes together with three additional spliceosome-related genes, including *U2AF65*, *SF1* and *SRSF1*, in a large series of myeloid neoplasms ($N = 582$) using a high-throughput mutation screen of pooled DNA followed by confirmation/identification of candidate mutations (refs 21 and 22 and Supplementary Methods II).

In total, 219 mutations were identified in 209 out of the 582 specimens of myeloid neoplasms through validating 313 provisional positive events in the pooled DNA screen (Supplementary Tables 4 and 5). The mutations among four genes, *U2AF35* ($N = 37$), *SRSF2* ($N = 56$), *ZRSR2* ($N = 23$) and *SF3B1* ($N = 79$), explained most of the mutations with much lower mutational rates for *SF3A1* ($N = 8$), *PRPF40B* ($N = 7$), *U2AF65* ($N = 4$) and *SF1* ($N = 5$) (Fig. 2). Mutations of the splicing machinery were highly specific to diseases showing myelodysplastic features, including MDS either with (84.9%) or without (43.9%) increased ring sideroblasts, chronic myelomonocytic leukaemia (CMML) (54.5%), and therapy-related AML or AML with myelodysplasia-related changes (25.8%), but were rare in *de novo* AML (6.6%) and myeloproliferative neoplasms (MPN) (9.4%) (Fig. 3a). The mutually exclusive pattern of the mutations in these splicing pathway genes was confirmed in this large case series, suggesting a common impact of these mutations on RNA splicing and the pathogenesis of myelodysplasia (Fig. 3b). The frequencies of mutations showed significant differences across disease types. Surprisingly, *SF3B1* mutations were found in the majority of the cases with MDS characterized by increased ring sideroblasts, that is, refractory anaemia with ring sideroblasts (RARS) (19/23 or 82.6%) and refractory cytopenia with multilineage dysplasia with ≥ 15% ring sideroblasts (RCMD-RS) (38/50 or 76%) with much lower mutation frequencies in other myeloid neoplasms. RARS and RCMD-RS account

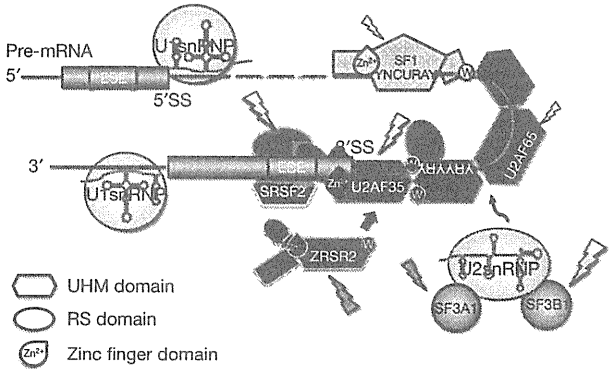

Figure 1 | Components of the splicing E/A complex mutated in myelodysplasia. RNA splicing is initiated by the recruitment of U1 snRNP to the 5′SS. SF1 and the larger subunit of the U2 auxiliary factor (U2AF), U2AF65, bind the branch point sequence (BPS) and its downstream polypyrimidine tract, respectively. The smaller subunit of U2AF (U2AF35) binds to the AG dinucleotide of the 3′SS, interacting with both U2AF65 and a SR protein, such as SRSF2, through its UHM and RS domain, comprising the earliest splicing complex (E complex). ZRSR2 also interacts with U2AF and SR proteins to perform essential functions in RNA splicing. After the recognition of the 3′SS, U2 snRNP, together with SF3A1 and SF3B1, is recruited to the 3′SS to generate the splicing complex A. The mutated components in myelodysplasia are indicated by arrows.

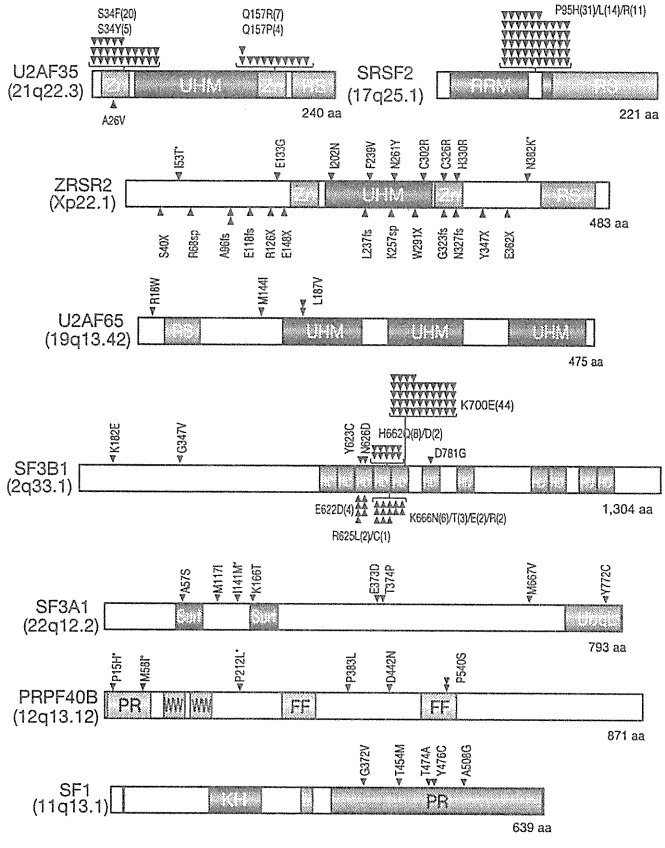

Figure 2 | Mutations of multiple components of the splicing machinery. Each mutation in the eight spliceosome components is shown with an arrowhead. Confirmed somatic mutations are discriminated by red arrows. Known domain structures are shown in coloured boxes as indicated. Mutations predicted as SNPs by MutationTaster (http://www.mutationtaster.org/) are indicated by asterisks. The number of each mutation is indicated in parenthesis. ZRSR2 mutations in females are shown in blue.

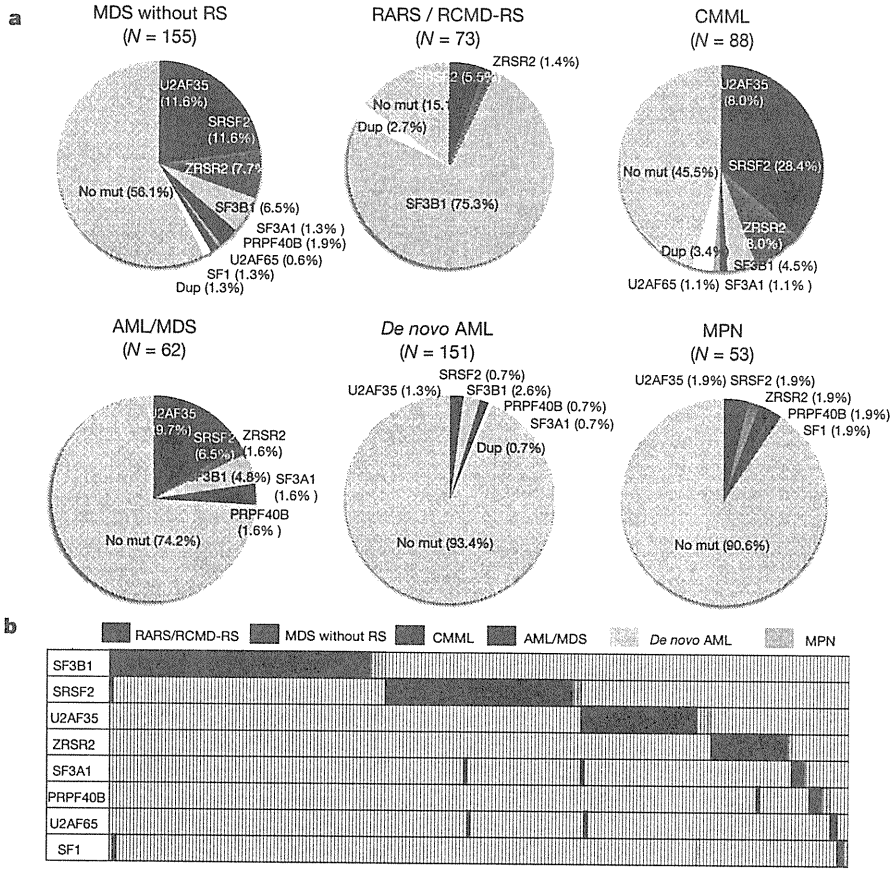

Figure 3 | Frequencies and distribution of spliceosome pathway gene mutations in myeloid neoplasms. **a**, Frequencies of spliceosome pathway mutations among 582 cases with various myeloid neoplasms. **b**, Distribution of mutations in eight spliceosome genes, where diagnosis of each sample is shown by indicated colours.

for 4.3% and 12.9% of MDS cases, respectively, where deregulated iron metabolism has been implicated in the development of refractory anaemia[23]. With such high mutation frequencies and specificity, the *SF3B1* mutations were thought to be almost pathognomonic to these MDS subtypes characterized by increased ring sideroblasts, and strongly implicated in the pathogenesis of MDS in these categories. Less conspicuously but significantly, *SRSF2* mutations were more frequent in CMML cases (Fig. 3 and Supplementary Table 4). Thus, although commonly involving the E/A splicing complexes, different mutations may still have different impacts on cell functions, contributing to the determination of discrete disease phenotypes. For example, studies have demonstrated that *SRSF2* was also involved in the regulation of DNA stability and that depletion of SRSF2 can lead to genomic instability[24]. Of interest in this context, regardless of disease subtypes, samples with *SRSF2* mutations were shown to have significantly more mutations of other genes compared with *U2AF35* mutations ($P = 0.001$, multiple regression analysis) (Supplementary Table 6 and Supplementary Fig. 7).

Notably, with a rare exception of A26V in a single case, the mutations of U2AF35 exclusively involved two highly conserved amino acid positions (S34 or Q157) within the amino- and the carboxyl-terminal zinc finger motifs flanking the U2AF homology motif (UHM) domain. SRSF2 mutations exclusively occurred at P95 within an intervening sequence between the RNA recognition motif (RRM) and arginine/serine-rich (RS) domains (Fig. 2 and Supplementary Figs 8 and 9). Similarly, SF3B1 mutations predominantly involved K700 and, to a lesser extent, K666, H662 and E622, which are also conserved across species (Fig. 2 and Supplementary Fig. 10). The involvement of recurrent amino acid positions in these spliceosome genes strongly indicated a gain-of-function nature of these mutations, which has been a well-documented scenario in other oncogenic mutations[25]. On the other hand, the 23 mutations in *ZRSR2* (Xp22.1) were widely distributed along the entire coding region (Fig. 2). Among these, 14 mutations were nonsense or frameshift changes, or involved splicing donor/acceptor sites that caused either a premature truncation or a large structural change of the protein, leading to loss-of-function. Combined with their strong male preference for the mutation (14/14 cases), *ZRSR2* most likely acts as a tumour suppressor gene with an X-linked recessive mode of genetic action. The remaining nine *ZRSR2* mutations were missense changes and found in both males (six cases) and females (three cases), whose somatic origin was only confirmed in two cases. However, neither the dbSNP database (build131 and 132) nor the 1000 Genomes database (May 2011 snp calls) contained these missense nucleotides, suggesting that many, if not all, of these missense changes are likely to represent functional somatic changes, especially those found in males. Interrogation of these hot spots for mutations in *U2AF35* and *SRSF2* found no mutations among lymphoid neoplasms, including acute lymphoblastic leukaemia ($N = 24$) or non-Hodgkin's lymphoma ($N = 87$) (data not shown).

RNA splicing and spliceosome mutations

Because the splicing pathway mutations in myelodysplasia widely and specifically affect the major components of the splicing complexes E/A in a mutually exclusive manner, the common consequence of these mutations is logically the impaired recognition of 3′SSs that would lead to the production of aberrantly spliced mRNA species. To appreciate this and also to gain an insight into the biological/biochemical impact of these splicing mutations, we expressed the wild-type and the mutant (S34F) U2AF35 in HeLa cells using retrovirus-mediated gene transfer with enhanced green fluorescent protein (EGFP) marking (Fig. 4a and Supplementary Methods III) and examined their effects on gene expression in these cells using GeneChip Human genome U133 plus 2.0 arrays (Affymetrix), followed by gene set enrichment analysis (GSEA) (Supplementary Methods IV)[26]. Intriguingly, the GSEA disclosed a significant enrichment of the genes on the nonsense-mediated mRNA decay (NMD) pathway among the significantly upregulated genes in mutant *U2AF35*-transduced HeLa cells (Fig. 4b, Supplementary Fig. 11a and Supplementary Table 7), which was

confirmed by quantitative polymerase chain reactions (qPCR) (Fig. 4c and Supplementary Methods 5V). A similar result was also observed for the gene expression profile of an MDS-derived cell line (TF-1) transduced with the S34F mutant (Supplementary Figs 11b, c). The NMD activation by the mutant U2AF35 was suppressed significantly by the co-overexpression of the wild-type protein (Supplementary Fig. 11d), indicating that the effect of the mutant protein was likely to be mediated by inhibition of the functions of the wild-type protein. Given that the NMD pathway, known as mRNA surveillance, provides a post-transcriptional mechanism for recognizing and eliminating abnormal transcripts that prematurely terminate translation[27], the result of the GSEA analyses indicated that the mutant U2AF35 induced abnormal RNA splicing in HeLa and TF-1 cells, leading to the generation of unspliced RNA species having a premature stop codon and induction of the NMD activity.

To confirm this, we next performed whole transcriptome analysis in these cells using the GeneChip Human exon 1.0 ST Array (Affymetrix), in which we differentially tracked the behaviour of two discrete sets of probes showing different level of evidence of being exons, that is, 'Core' (authentic exons) and 'non-Core' (more likely introns) sets (Supplementary Methods IV and Supplementary Fig. 12). As shown in Fig. 4d, the Core and non-Core set probes were differentially enriched among probes showing significant difference in expression between wild-type and mutant-transduced cells (false discovery rate (FDR) = 0.01). The Core set probes were significantly enriched in those probes significantly downregulated in mutant *U2AF35*-transduced cells compared with wild-type *U2AF35*-transduced cells, whereas the non-Core set probes were enriched in those probes significantly upregulated in mutant *U2AF35*-transduced cells (Fig. 4e). The significant differential enrichment was also demonstrated, even when all probe sets were included (Fig. 4f). Moreover, the significantly differentially expressed Core set probes tended to be up- and downregulated in wild-type and mutant *U2AF35*-transduced cells compared with mock-transduced cells, respectively, and vice versa for the differentially expressed non-Core set probes (Fig. 4e). Combined, these exon array results indicated that the wild-type U2AF35 correctly promoted authentic RNA splicing, whereas the mutant U2AF35 inhibited this processes, rendering non-Core and therefore, more likely intronic sequences to remain unspliced.

The abnormal splicing in mutant *U2AF35*-transduced cells was more directly demonstrated by sequencing mRNAs extracted from HeLa cells, in which expression of the wild-type and mutant (S34F) U2AF35 were induced by doxycycline. First, after adjusting by the total number of mapped reads, the wild-type *U2AF35*-transduced cells showed an increased read counts in the exon fraction, but reduced counts in other fractions, compared with mutant *U2AF35*-transduced cells (Fig. 4g). The reads from the mutant-transduced cells were mapped to broader genomic regions compared with those from the wild-type *U2AF35*-transduced cells, which were largely explained by non-exon reads (Fig. 4h). Finally, the number of those reads that encompassed the authentic exon/intron junctions was significantly increased in mutant *U2AF35*-transduced cells compared with wild-type *U2AF35*-transduced cells (Fig. 4i and Supplementary Methods VI). These results clearly demonstrated that failure of splicing ubiquitously occurred in mutant *U2AF35*-transduced cells. A typical example of abnormal splicing in mutant-transduced cells and the list of significantly unspliced exons are shown in Supplementary Fig. 13 and Supplementary Table 8, respectively.

Biological consequence of U2AF35 mutations

Finally, we examined the biological effects of compromised functions of the E/A splicing complexes. First, TF-1 and HeLa cells were transduced with lentivirus constructs expressing either the S34F U2AF35 mutant or wild-type U2AF35 under a tetracycline-inducible promoter (Fig. 5a and Supplementary Figs 14a and 15a), and cell proliferation was examined after the induction of their expression. Unexpectedly, after the induction of gene expression with doxycycline, the mutant *U2AF35*-transduced cells, but not the wild-type *U2AF35*-transduced cells, showed reduced cell proliferation (Fig. 5b and Supplementary Fig. 15b) with a marked increase in the G2/M fraction (G2/M arrest) together with enhanced apoptosis as

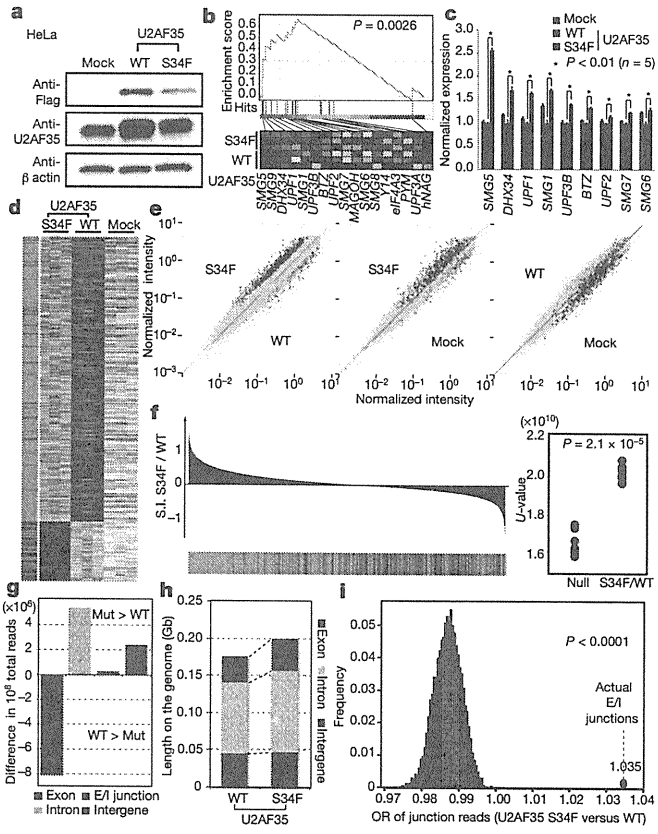

Figure 4 | Altered RNA splicing caused by a U2AF35 mutant. **a**, Western blot analyses showing expression of transduced wild-type or mutant (S34F) U2AF35 in HeLa cells used for the analyses of expression and exon microarrays. **b**, The GSEA demonstrating a significant enrichment of the set of 17 NMD pathway genes among significantly differentially expressed genes between wild-type and mutant *U2AF35*-transduced HeLa cells. The significance of the gene set was empirically determined by 1,000 gene-set permutations. **c**, The confirmation of the microarray analysis for the expression of nine genes that contributed to the core enrichment in the NMD gene set. Means ± s.e. are provided for the indicated NMD genes. *P* values were determined by the Mann–Whitney *U* test. **d**, Significantly upregulated and downregulated probe sets (FDR = 0.01) in mutant *U2AF35*-transduced cells compared with wild-type *U2AF35*-transduced cells in triplicate exon array experiments are shown in a heat map. The origin of each probe set is depicted in the left lane, where red and green bars indicate the Core and non-Core sets, respectively. **e**, Pair-wise scatter plots of the normalized intensities of entire probe sets (grey) across different experiments. The Core and non-Core set probes that were significantly differentially expressed between the wild-type and mutant *U2AF35*-transduced cells are plotted in red and green, respectively. **f**, Distribution of the Core (red) and non-Core (green) probe sets within the entire probe sets ordered by splicing index (S.I.; Supplementary Methods IV), calculated between wild-type and mutant *U2AF35*-transduced cells. In the right panel, the differential enrichment of both probe sets was confirmed by Mann–Whitney *U* test. **g**, Difference in read counts for the indicated fractions per 10^8 total reads in RNA sequencing between wild-type and mutant U2AF35-expressing HeLa cells analysis. Increased/decreased read counts in mutant U2AF35-expressing cells are plotted upward/downward, respectively. **h**, Comparison of the genome coverage by the indicated fractions in wild-type- and mutant-U2AF35-expressing cells. The genome coverage was calculated for each fraction within the 10^8 reads randomly selected from the total reads and averaged for ten independent selections. **i**, The odds ratio of the junction reads within the total mapped reads was calculated between the two experiments (red circle), which was evaluated against the 10,000 simulated values under the null hypothesis (histogram in blue).

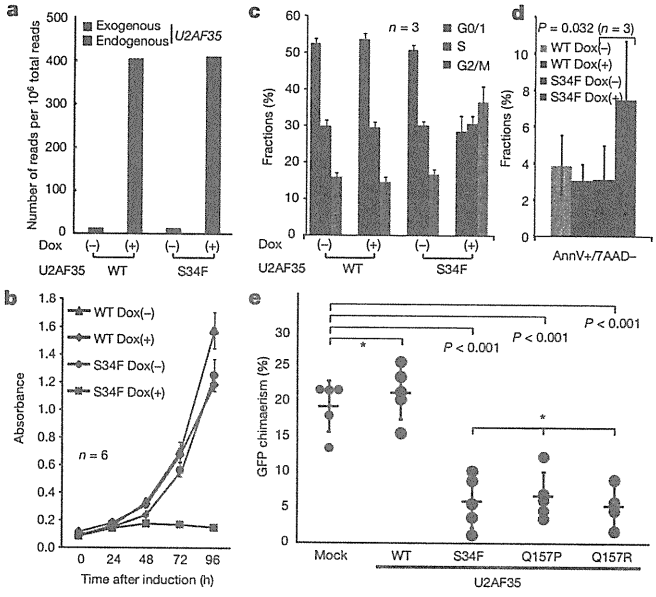

Figure 5 | Functional analysis of mutant U2AF35. **a**, Expression of endogenous and exogenous *U2AF35* transcripts in HeLa cells before and after induction determined by RNA sequencing. *U2AF35* transcripts were differentially enumerated for endogenous and exogenous species, which were discriminated by the Flag sequence. **b**, Cell proliferation assays of *U2AF35*-transduced HeLa cells, where cell numbers were measured using cell-counting apparatus and are plotted as mean absorbance ± s.d. **c**, The flow cytometry analysis of propidium iodide (PI)-stained HeLa cells transduced with the different U2AF35 constructs. Mean fractions ± s.d. in G0/G1, S and G2/M populations after the induction of U2AF35 expression are plotted. **d**, Fractions of the annexin V-positive (AnnV+) populations among the 7-amino-actinomycin D (7AAD)-negative population before and after the induction of U2AF35 expression are plotted as mean ± s.d. for indicated samples. The significance of difference was determined by paired *t*-test. **e**, Competitive reconstitution assays for CD34-negative KSL cells transduced with indicated U2AF35 mutants. Chimaerism in the peripheral blood 6 weeks after transplantation are plotted as mean %EGFP-positive Ly5.1 cells ± s.d., where outliers were excluded from the analysis. The significance of differences was evaluated by the Grubbs test with Bonferroni's correction for multiple testing. *not significant.

indicated by the increased sub-G1 fraction and annexin V-positive cells (Fig. 5c, d, Supplementary Fig. 14b and Supplementary Methods VI). To confirm the growth-suppressive effect of U2AF35 mutants *in vitro*, a highly purified haematopoietic stem cell population ($CD34^-c\text{-}Kit^+Scal^+Lin^-$, $CD34^-KSL$) prepared from C57BL/6 (B6)-Ly5.1 mouse bone marrow[28] was retrovirally transduced with either the mutant (S34F, Q157P and Q157R) or wild-type *U2AF35*, or the mock constructs, each harbouring the EGFP marker gene (Supplementary Fig. 16). The ability of these transduced cells to reconstitute the haematopoietic system was tested in a competitive reconstitution assay. The transduced cells were mixed with whole bone marrow cells from B6-Ly5.1/5.2 F1 mice, transplanted into lethally irradiated B6-Ly5.2 recipients, and peripheral blood chimaerism derived from EGFP-positive cells was assessed 6 weeks after transplantation by flow cytometry. We confirmed that each recipient mouse received comparable numbers of EGFP-positive cells among the different retrovirus groups by estimating the percentage of EGFP-positive cells and overall proliferation in transduced cells by *ex vivo* tracking. Also no significant difference was observed in their homing capacity to bone marrow as assessed by transwell migration assays (Supplementary Fig. 17). As shown in Fig. 5e, the wild-type *U2AF35*-transduced cells showed a slightly higher reconstitution capacity than the mock-transduced cells. On the other hand, the recipients of the cells transduced with the various *U2AF35* mutants showed significantly lower EGFP-positive cell chimaerism than those of either the mock- or the wild-type *U2AF35*-transduced cells, indicating a compromised reconstitution capacity of the haematopoietic stem/progenitor cells expressing the U2AF35 mutants. In summary, these mutants lead to loss-of-function of U2AF35 most probably by acting in a dominant-negative fashion to the wild-type protein.

Discussion

Our whole-exome sequencing study unexpectedly unmasked a complexity of novel pathway mutations found in approximately 45% to 85% of myelodysplasia patients depending on the disease subtypes, which affected multiple but distinctive components of the splicing machinery and, as such, demonstrated the unquestionable power of massively parallel sequencing technologies in cancer research.

The RNA splicing system comprises essential cellular machinery, through which eukaryotes can achieve successful transcription and guarantee the functional diversity of their protein species using alternative splicing in the face of a limited number of genes[29]. Accordingly, the meticulous regulation of this machinery should be indispensable for the maintenance of cellular homeostasis[30], deregulation of which causes severe developmental abnormalities[31,32]. The current discovery of frequent mutations of the splicing pathway in myelodysplasia, therefore, represents another remarkable example that illustrates how cancer develops by targeting critical cellular functions. It also provides an intriguing insight into the mechanism of 'cancer specific' alternative splicing, which have long been implicated in the development of cancer, including MDS and other haematopoietic neoplasms[33,34].

In myelodysplasia, the major targets of spliceosome mutations seemed to be largely confined to the components of the E/A splicing complex, among others to *SF3B1*, *SRSF2*, *U2AF35* and *ZRSR2*, and to a lesser extent, to *SF3A1*, *SF1*, *U2AF65* and *PRPF40B*. The broad coverage of the wide spectrum of spliceosome components in our exome sequencing was likely to preclude frequent involvement of other components on this pathway (Supplementary Fig. 18). The surprising frequency and specificity of these mutations in this complex, together with the mutually exclusive manner they occurred, unequivocally indicate that the compromised function of the E/A complex is a hallmark of this unique category of myeloid neoplasms, playing a central role in the pathogenesis of myelodysplasia. The close relationship between the mutation types and unique disease subtypes also support their pivotal roles in MDS.

Given the critical functions of the E/A splicing complex on the precise 3′SS recognition, the logical consequence of these relevant mutations would be the impaired splicing involving diverse RNA species. In fact, when expressed in HeLa cells, the mutant U2AF35 induced global abnormalities of RNA splicing, leading to increased production of transcripts having unspliced intronic sequences. On the other hand, the functional link between the abnormal splicing of RNA species and the phenotype of myelodysplasia is still unclear. Mutant U2AF35 seemed to suppress cell growth/proliferation and induce apoptosis rather than confer a growth advantage or promote clonal selection. *ZRSR2* knockdown in HeLa cells has been reported to also result in reduced viability, arguing for the common consequence of these pathway mutations[35]. These observations suggested that the oncogenic actions of these splicing pathway mutations are distinct from what is expected for classical oncogenes, such as mutated kinases and signal transducers, but could be more related to cell differentiation. Of note in this regard, the commonest clinical presentation of MDS is severe cytopenia in multiple cell lineages due to ineffective haematopoiesis with increased apoptosis rather than unlimited cell proliferation[1]. In this regard, lessons may be learned from the recent findings on the pathogenesis of the 5q− syndrome, where haploinsufficiency of *RPS14* leads to increased apoptosis of erythroid progenitors, but not myeloproliferation[36,37].

A lot of issues remain to be answered, however, to establish the functional link between these splicing pathway mutations and the

pathogenesis of MDS, where the broad spectrum of RNA species affected by impaired splicing hampers identification of responsible gene targets. Moreover, the mutated components of the splicing machinery have distinct function of their own other than direct regulation of RNA splicing, involved in elongation and DNA stability, which may be important to determine specific disease phenotypes. Clearly, more studies are required to answer these questions through understanding of the molecular basis of their oncogenic actions.

METHODS SUMMARY

Whole-exome sequencing of paired tumour/normal DNA samples from the 29 patients was performed after informed consent was obtained. SNP array-based copy number analysis was performed as previously described[17,18]. Mutation analysis of the splicing pathway genes in a set of 582 myeloid neoplasms were performed by first screening mutations in PCR-amplified pooled targets from 12 individuals, followed by validation/identification of the candidate mutations within the corresponding 12 individuals by Sanger sequencing. Flag-tagged cDNAs of the wild-type and mutant *U2AF35* were generated by *in vitro* mutagenesis, constructed into a murine stem cell virus-based retroviral vector as well as a tetracycline-inducible lentivirus-based expression vector, and used for gene transfer to $CD34^{-}$KSL cells and cultured cell lines, with EGFP marking, respectively. Total RNA was extracted from wild-type or mutant *U2AF35*-transduced HeLa and TF-1 cells, and analysed on microarrays. RNA sequencing was performed according to the manufacturer's instructions (Illumina). Cell proliferation assays (MTT assays) on HeLa and TF-1 cells stably transduced with lentivirus U2AF35 constructs were performed in the presence or absence of doxycycline. For competitive reconstitution assays, $CD34^{-}$KSL cells collected from C57BL/6 (B6)-Ly5.1 mice were retrovirally transduced with various *U2AF35* constructs with EGFP marking, and transplanted with competitor cells (B6-Ly5.1/5.2 F1 mouse origin) into lethally irradiated B6-Ly5.2 mice 48 h after gene transduction. Frequency of EGFP-positive cells was assessed in peripheral blood by flow cytometry 6 weeks after the transplantation (Supplementary Methods VII). The primer sets used for validation of gene mutations and qPCR of NMD gene expression are listed in Supplementary Tables 9–11. A complete description of the materials and methods is provided in the Supplementary Information. This study was approved by the ethics boards of the University of Tokyo, Munich Leukaemia Laboratory, University Hospital Mannheim, University of Tsukuba, Tokyo Metropolitan Ohtsuka Hospital and Chang Gung Memorial Hospital. Animal experiments were performed with approval of the Animal Experiment Committee of the University of Tokyo.

Received 7 June; accepted 24 August 2011.
Published online 11 September 2011.

1. Corey, S. J. *et al.* Myelodysplastic syndromes: the complexity of stem-cell diseases. *Nature Rev. Cancer* **7,** 118–129 (2007).
2. Ma, X., Does, M., Raza, A. & Mayne, S. T. Myelodysplastic syndromes: incidence and survival in the United States. *Cancer* **109,** 1536–1542 (2007).
3. Bejar, R., Levine, R. & Ebert, B. L. Unraveling the molecular pathophysiology of myelodysplastic syndromes. *J. Clin. Oncol.* **29,** 504–515 (2011).
4. Sanada, M. *et al.* Gain-of-function of mutated *C-CBL* tumour suppressor in myeloid neoplasms. *Nature* **460,** 904–908 (2009).
5. Campbell, P. J. *et al.* Identification of somatically acquired rearrangements in cancer using genome-wide massively parallel paired-end sequencing. *Nature Genet.* **40,** 722–729 (2008).
6. Chapman, M. A. *et al.* Initial genome sequencing and analysis of multiple myeloma. *Nature* **471,** 467–472 (2011).
7. Lee, W. *et al.* The mutation spectrum revealed by paired genome sequences from a lung cancer patient. *Nature* **465,** 473–477 (2010).
8. Ley, T. J. *et al.* DNA sequencing of a cytogenetically normal acute myeloid leukaemia genome. *Nature* **456,** 66–72 (2008).
9. Metzker, M. L. Sequencing technologies — the next generation. *Nature Rev. Genet.* **11,** 31–46 (2010).
10. Shendure, J. & Ji, H. Next-generation DNA sequencing. *Nature Biotechnol.* **26,** 1135–1145 (2008).
11. Shah, S. P. *et al.* Mutational evolution in a lobular breast tumour profiled at single nucleotide resolution. *Nature* **461,** 809–813 (2009).
12. Varela, I. *et al.* Exome sequencing identifies frequent mutation of the SWI/SNF complex gene *PBRM1* in renal carcinoma. *Nature* **469,** 539–542 (2011).
13. Ley, T. J. *et al. DNMT3A* mutations in acute myeloid leukemia. *N. Engl. J. Med.* **363,** 2424–2433 (2010).
14. Mardis, E. R. *et al.* Recurring mutations found by sequencing an acute myeloid leukemia genome. *N. Engl. J. Med.* **361,** 1058–1066 (2009).
15. Yan, X. J. *et al.* Exome sequencing identifies somatic mutations of DNA methyltransferase gene *DNMT3A* in acute monocytic leukemia. *Nature Genet.* **43,** 309–315 (2011).
16. Puente, X. S. *et al.* Whole-genome sequencing identifies recurrent mutations in chronic lymphocytic leukaemia. *Nature* **475,** 101–105 (2011).
17. Nannya, Y. *et al.* A robust algorithm for copy number detection using high-density oligonucleotide single nucleotide polymorphism genotyping arrays. *Cancer Res.* **65,** 6071–6079 (2005).
18. Yamamoto, G. *et al.* Highly sensitive method for genomewide detection of allelic composition in nonpaired, primary tumor specimens by use of Affymetrix single-nucleotide-polymorphism genotyping microarrays. *Am. J. Hum. Genet.* **81,** 114–126 (2007).
19. Wahl, M. C., Will, C. L. & Luhrmann, R. The spliceosome: design principles of a dynamic RNP machine. *Cell* **136,** 701–718 (2009).
20. Tronchère, H., Wang, J. & Fu, X. D. A protein related to splicing factor $U2AF^{35}$ that interacts with $U2AF^{65}$ and SR proteins in splicing of pre-mRNA. *Nature* **388,** 397–400 (1997).
21. Bevilacqua, L. *et al.* A population-specific *HTR2B* stop codon predisposes to severe impulsivity. *Nature* **468,** 1061–1066 (2010).
22. Calvo, S. E. *et al.* High-throughput, pooled sequencing identifies mutations in *NUBPL* and *FOXRED1* in human complex I deficiency. *Nature Genet.* **42,** 851–858 (2010).
23. Haase, D. *et al.* New insights into the prognostic impact of the karyotype in MDS and correlation with subtypes: evidence from a core dataset of 2124 patients. *Blood* **110,** 4385–4395 (2007).
24. Xiao, R. *et al.* Splicing regulator SC35 is essential for genomic stability and cell proliferation during mammalian organogenesis. *Mol. Cell. Biol.* **27,** 5393–5402 (2007).
25. Morin, R. D. *et al.* Somatic mutations altering EZH2 (Tyr641) in follicular and diffuse large B-cell lymphomas of germinal-center origin. *Nature Genet.* **42,** 181–185 (2010).
26. Subramanian, A. *et al.* Gene set enrichment analysis: a knowledge-based approach for interpreting genome-wide expression profiles. *Proc. Natl Acad. Sci. USA* **102,** 15545–15550 (2005).
27. Maquat, L. E. Nonsense-mediated mRNA decay: splicing, translation and mRNP dynamics. *Nature Rev. Mol. Cell Biol.* **5,** 89–99 (2004).
28. Ema, H. *et al.* Adult mouse hematopoietic stem cells: purification and single-cell assays. *Nature Protocols* **1,** 2979–2987 (2007).
29. Chen, M. & Manley, J. L. Mechanisms of alternative splicing regulation: insights from molecular and genomics approaches. *Nature Rev. Mol. Cell Biol.* **10,** 741–754 (2009).
30. Ni, J. Z. *et al.* Ultraconserved elements are associated with homeostatic control of splicing regulators by alternative splicing and nonsense-mediated decay. *Genes Dev.* **21,** 708–718 (2007).
31. He, H. *et al.* Mutations in U4atac snRNA, a component of the minor spliceosome, in the developmental disorder MOPD I. *Science* **332,** 238–240 (2011).
32. Edery, P. *et al.* Association of TALS developmental disorder with defect in minor splicing component *U4atac* snRNA. *Science* **332,** 240–243 (2011).
33. David, C. J. & Manley, J. L. Alternative pre-mRNA splicing regulation in cancer: pathways and programs unhinged. *Genes Dev.* **24,** 2343–2364 (2010).
34. Pajares, M. J. *et al.* Alternative splicing: an emerging topic in molecular and clinical oncology. *Lancet Oncol.* **8,** 349–357 (2007).
35. Shen, H., Zheng, X., Luecke, S. & Green, M. R. The U2AF35-related protein Urp contacts the 3′ splice site to promote U12-type intron splicing and the second step of U2-type intron splicing. *Genes Dev.* **24,** 2389–2394 (2010).
36. Barlow, J. L. *et al.* A p53-dependent mechanism underlies macrocytic anemia in a mouse model of human 5q− syndrome. *Nature Med.* **16,** 59–66 (2010).
37. Ebert, B. L. *et al.* Identification of *RPS14* as a $5q^{-}$ syndrome gene by RNA interference screen. *Nature* **451,** 335–339 (2008).

Supplementary Information is linked to the online version of the paper at www.nature.com/nature.

Acknowledgements This work was supported by Grant-in-Aids from the Ministry of Health, Labor and Welfare of Japan and from the Ministry of Education, Culture, Sports, Science and Technology, and also by the Japan Society for the Promotion of Science (JSPS) through the 'Funding Program for World-Leading Innovative R&D on Science and Technology (FIRST Program)', initiated by the Council for Science and Technology Policy (CSTP). pGCDNsamIRESEGFP vector was a gift from M. Onodera. We thank Y. Mori, O. Hagiwara, M. Nakamura and N. Mizota for their technical assistance. We are also grateful to K. Ikeuchi and M. Ueda for their continuous encouragement throughout the study.

Author Contributions Y.Sh., Y.Sa., A.S.-O., Y.N., M.N., G.C., R.K. and S.Miyano were committed to bioinformatics analyses of resequencing data. M.Sa., A.S.-O. and Y.Sa. performed microarray experiments and their analyses. R.Y., T.Y., M.O., M.Sa., A.K., M.Sh. and H.N. were involved in the functional analyses of U2AF35 mutants. N.O., M.S.-Y., K.I., H.M., W.-K.H., F.N., D.N., T.H., C.H., S.Miyawaki, S.C., H.P.K. and L.-Y.S. collected specimens and were also involved in planning the project. K.Y., Y.N., Y.Su., A.S.-O. and S.S. processed and analysed genetic materials, library preparation and sequencing. K.Y., M.Sa., Y.Sh., A.S.-O., Y. Sa. and S.O. generated figures and tables. S.O. led the entire project and wrote the manuscript. All authors participated in the discussion and interpretation of the data and the results.

Author Information Sequence data have been deposited in the DDBJ repository under accession number DRA000433. Microarray data have been deposited in the GEO database under accession numbers GSE31174 (for SNP arrays), GSE31171 (for exon arrays) and GSE31172 (for expression arrays). Reprints and permissions information is available at www.nature.com/reprints. The authors declare no competing financial interests. Readers are welcome to comment on the online version of this article at www.nature.com/nature. Correspondence and requests for materials should be addressed to S.O. (sogawa-tky@umin.ac.jp).

J Clin Exp Hematopathol
Vol. 51, No. 2, Nov. 2011

Original Article

Treatment Outcome of Adult Burkitt Lymphoma in Japanese Patients with Modified LMB Protocol : A Single Center Retrospective Analysis

Hidekazu Nishikii,[1] Naoya Nakamura,[2] Yuzuru Kondo,[3] Yasushi Okoshi,[1] Kazumi Suzukawa,[1] Yuichi Hasegawa,[1] Yasuhisa Yokoyama,[1] Mamiko Sakata-Yanagimoto,[1] Terukazu Enami,[1] Masayuki Noguchi,[3] and Shigeru Chiba[1]

The prognosis of adult Burkitt lymphoma (BL) has improved in western countries since the introduction of high-dose methotrexate (HD-MTX)-containing chemotherapy. Here we analyzed nine consecutive Japanese patients diagnosed with BL at our institution. All except for the three elderly (> 70 years) patients were treated with a regimen including 13 g/m^2 HD-MTX in total, divided into 3 cycles. The median follow-up period was 56 months (range 38-118). All the nine patients achieved complete remission and have not shown any disease progression, including the three elderly patients who received reduced doses or alternative treatments. These observations suggest that chemotherapy including 13 g/m^2 HD-MTX in total is tolerable and effective in Japanese adult BL patients aged < 70 and that BL is curable even if developed in those who are > 70 years. [*J Clin Exp Hematopathol 51(2) : 109-114, 2011*]

Keywords: Burkitt lymphoma, high-dose methotrexate, World Health Organization classification

INTRODUCTION

Burkitt lymphoma (BL) is a rare, highly aggressive B-cell lymphoma that preferentially occurs in children and young adults.[1,2] Despite its highly aggressive course, the prognosis of BL has improved after the introduction of rapidly cycling, intensive chemotherapy regimens such as the "LMB (Lymphoma Malignancy B) protocol" (originally reported by a French group) and "CODOX-M/IVAC (cyclophosphamide, vincristine, doxorubicin, methotrexate/ifosfamide, etoposide, and cytrabine) therapy" that include high-dose methotrexate (HD-MTX).[3-5] However, most of the studies testing these regimens were performed in European and North American populations and their suitability for other populations remains to be determined.

Here, we report, after re-evaluation of diagnosis based on version 4 (v4) of the World Health Organization (WHO) classification, a retrospective analysis of eleven consecutive Japanese patients who were diagnosed with BL or B-cell lymphoma, unclassifiable, with features intermediate between diffuse large B-cell lymphoma and Burkitt lymphoma (iDLBCL/BL) and treated with an LMB-like regimen.

Received : April 1, 2011
Revised : July 7, 2011
Accepted : August 19, 2011
[1]Department of Hematology, Graduate School of Comprehensive Human Sciences, University of Tsukuba, Tsukuba, Ibaraki, Japan
[2]Department of Pathology, Tokai University School of Medicine, Isehara, Kanagawa, Japan
[3]Department of Pathology, Graduate School of Comprehensive Human Sciences, University of Tsukuba, Tsukuba, Ibaraki, Japan
Address correspondence and reprint requests to : Shigeru Chiba, M. Ph.D.Department of Hematology, University of Tsukuba, 1-1-1, Tennoudai, Tsukuba, Ibaraki 305-8575, Japan
E-mail : schiba-t@md.tsukuba.ac.jp

PATIENTS AND METHODS

Patients and re-evaluation

We reviewed the clinical records at Tsukuba University Hospital between 1996 and 2009, and identified 12 and 1 patients who, according to the v3 WHO classification, had been diagnosed with BL and Burkitt-like lymphoma (BLL), respectively (Table 1). One BL patient diagnosed in 1996 was excluded from this analysis because he received allogeneic stem cell transplantation after chemotherapy. Another BL patient was positive for human immunodeficiency virus (HIV) and was also excluded from the analysis. Thus, 10 BL and 1 BLL consecutive cases, all of which were negative for HIV, were re-evaluated for diagnosis on the basis of the v4

Table 1. Clinical features, diagnosis according to the v3 WHO classification, stage, and survival of the patients

Case No.	Age/Sex	Main lesion	Bulky	CNS	BM	Stage	PS ≥ 2	Initial diagnosis	CR	Current status	Follow up period (months)
1	46/F	jaw, stomach	+	-	-	III	Yes	BL	Yes	Alive	118
2	70/M	salivary gland	+	-	-	II	Yes	BL	Yes	Alive	112
3	65/F	salivary gland, stomach	+	-	-	III	Yes	BL	Yes	Alive	103
4	73/M	salivary gland	+	-	+	IV	Yes	BL	Yes	Alive	38
5	16/M	paraaorta, axillary	+	+	-	IV	No	BL	Yes	Alive	56
6	20/F	ovary, paraaorta	+	-	-	IV	Yes	BL	Yes	Alive	56
7	82/M	paraaorta, mediastinum	+	-	+	III	Yes	BL	Yes	Alive	41
8	54/M	pharynx	-	-	-	I	Yes	BL	Yes	Alive	38
9	40/F	ovary, paraaorta	+	-	-	III	No	BL	Yes	Alive	60
10	39/F*	ovary, paraaorta	+	-	-	IV	Yes	BLL	No	Death	3
11	42/M*	salivary gland, stomach	+	+	-	IV	Yes	BL	Yes	CNS relapse Death	7

The clinical stage of each case was defined by the Ann Arbor staging system. BL; Burkitt lymphoma, BLL; Burkitt-like lymphoma,*; Two patients were diagnosed as iDLBCL/BL after re-evaluation according to the v4 classification.

WHO classification.

For the re-evaluation, hematoxylin-eosin-stained specimens were reviewed by two pathologists who were not involved in the initial diagnosis. Immunocytochemical stainings of paraffin sections were added to evaluate the expression of CD10, CD20, BCL2, BCL6, MUM1, and Ki-67. Rearrangement of the *cMYC* and *BCL2* genes was studied by interphase fluorescence *in situ* hybridization (FISH) on thin-sliced paraffin sections. The probes used for FISH were Dual Fusion Translocation Probe IGH SG/MYC SO [for t(8;14); Vysis, Richmond, United Kingdom], BCL2 FISH DNA Probe Split Signal and MYC FISH DNA Probe Split Signal [for (14;18), and t(8;14) and t(2;8), respectively; DAKO, Carpinteria, CA, USA].[6]

The clinical stage of each case was defined by the Ann Arbor staging system. The bulky mass was defined as a tumor with a diameter of at least 10 cm.

Treatment

The 6BL patients who were < 70 years, as well as 2 iDLBCL/BL patients, were treated with intensive chemotherapy based on the LMB protocol as summarized in Fig. 1 (modified LMB protocol).[7-10] The doses of cyclophosphamide (CPA) in induction therapy, and cytrabine (AraC) and etoposide (VP-16) in consolidation #1 were reduced compared with those in the original LMB protocol. AraC in original consolidation #2 was also changed to VP-16 on days 3-6.[10] The induction regimen consisted of MTX (5,000 mg/m^2) on day 1, CPA (1,000 mg/m^2) on days 2 and 3, adriamycin (ADR, 60 mg/m^2) on day 2, vincristine (VCR, 1.4 mg/m^2) on days 1 and 7, prednisolone (PSL, 60 mg/m^2) on days 1-10, and granulocyte colony-stimulating factor (G-CSF, 5 μg/m^2) on day 5, which was continued until absolute white blood cell count of > 5.0 × 10^3/mL with > 50% neutrophils was achieved. As CNS prophylaxis, intrathecal therapy (IT) consisting of AraC (40 mg), MTX (15 mg), and PSL (20 mg) was applied on day 1. CNS prophylactic irradiation was not included at any point in the treatment plan. Leukovorin rescue was commenced 2 hr after the completion of HD-MTX administration and continued until the serum MTX level was decreased to < 5 × 10^{-8} M. This regimen was repeated once for all patients. The 3 elderly BL patients principally received the same regimen except that the dose of MTX was reduced to 1,000 mg/m^2. To keep the intervals between regimens as short as possible, the next regimen was started when absolute neutrophil counts of > 1.5 × 10^3/mL and platelet counts of > 10 × 10^4/mL were achieved. For patients with a bulky mass or a poor general condition, prephase therapy with PSL alone, COP (CPA, VCR, and PSL), or CHOP (CPA, VCR, ADR, and PSL) was performed before induction therapy.

After complete remission (CR) or uncertain remission (CRu) was confirmed, and if absolute neutrophil and platelet counts were over 1.5 × 10^3/mL and 10 × 10^4/mL, respectively, the consolidation #1 regimen was started. This regimen consisted of IT on days 1 and 6, AraC (2,000 mg/m^2 × 2) on days 3-5, and VP-16 (100 mg/m^2) on days 3-6. Rituximab (375 mg/m^2) was added to the consolidation #1 regimen (on day 1) for patients who were diagnosed after April, 2006.

If absolute neutrophil and platelet counts were over 1.5 × 10^3/mL and 10 × 10^4/mL, respectively, the consolidation #2 regimen was started. This regimen consisted of IT on days 1 and 6, MTX (3,000 mg/m^2) on day 3, and VP-16 (60 mg/m^2) on days 3-6. Rituximab (375 mg/m^2) was added to the consolidation #2 regimen (on day 1) for patients who were diagnosed after April, 2006. G-CSF was used during neutropenia (< 500/mm^3).

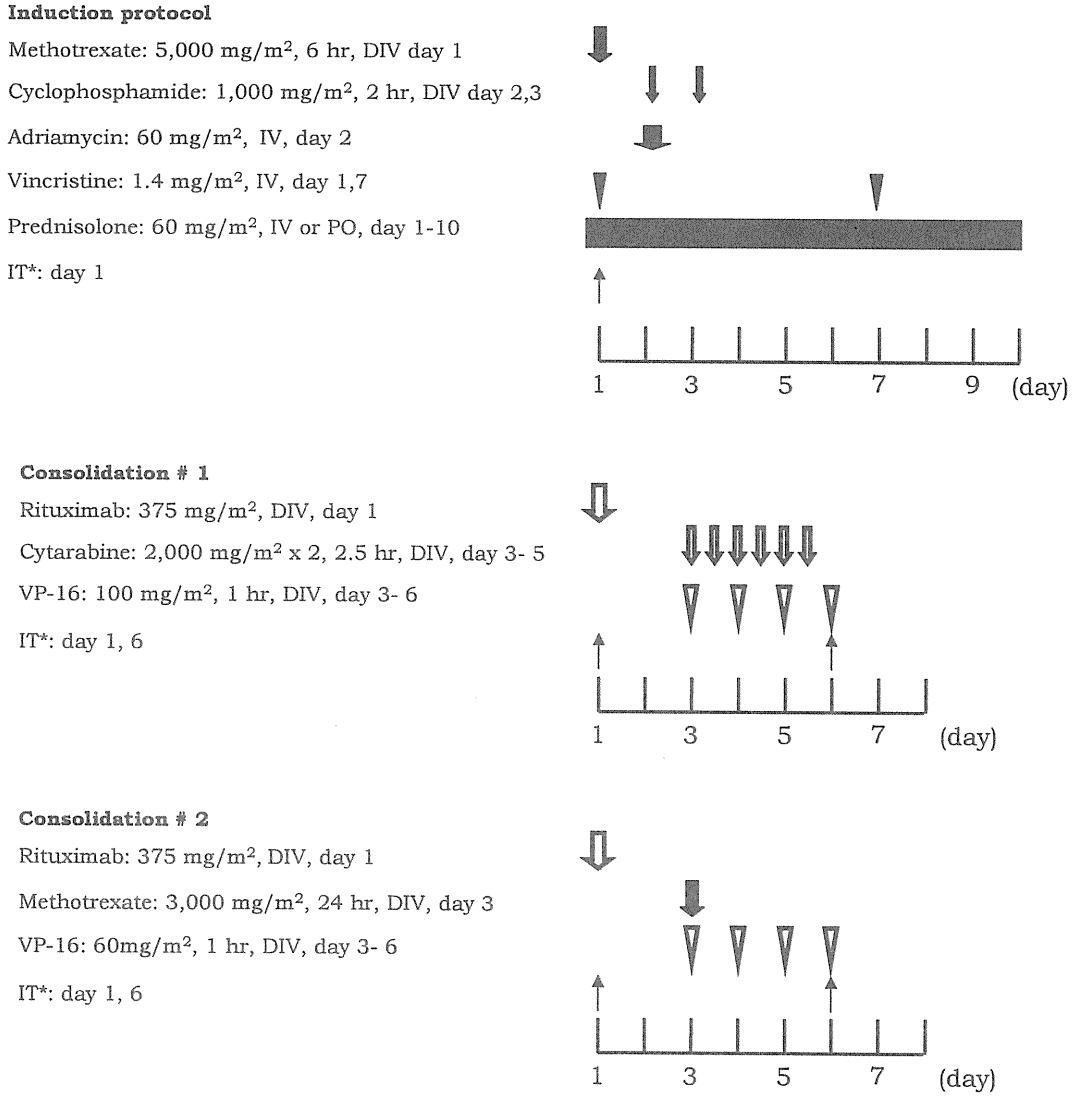

Fig. 1. Treatment scheme. The induction course was repeated once (2 induction courses in total). IV, intravenous injection; PO, orally; IT*, intrathecal chemotherapy (cytarabine 40 mg + methotrexate 15 mg + prednisolone 20 mg)

Assessment of remission and adverse events

Initial staging and prognosis factors were evaluated by obtaining a medical history, performing a physical examination and standard blood tests, including measurements of lactate dehydrogenase (LDH) and soluble interleukin-2 receptor (sIL-2R) levels, and conducting other examinations as follows: computed tomographic scan of the chest, abdomen, and pelvis; magnetic resonance imaging of the brain and spine; lumbar puncture [if central nervous system (CNS) involvement was suspected]; and bone marrow aspiration and biopsy. All cases were examined for anti-HIV antibody, hepatitis B surface (HBs) antigen, anti-HBs antibody, and hepatitis C antibody. Elevated serum LDH and sIL-2R levels were defined when greater than 245 U/L and 519 U/mL, respectively. Responses were evaluated according to the guidelines reported by Cheson *et al.*[11] Toxicities and adverse events related to chemotherapy were assessed and graded according to the National Cancer Institute Common Toxicity Criteria, version 2.0.[12]

RESULTS

Re-evaluation based on the v4 WHO classification

The median age of patients was 46 years (range 16-82),

Table 2. Diagnosis and re-evaluation of the patients according to the v4 classification

Case No.	Age/Sex	Starry sky	Ki-67	CD10	CD20	BCL2	BCL6	MUM1	*IgH/ cMYC*	cMYC split	BCL2 split	G-band	Initial diagnosis (v3)	Reviewed diagnosis (v4)
1	46/F	+	≧ 90%	+	+	-	+	-	+	+	-	N. D*	BL	BL
2	70/M	+	≧ 90%	+	+	-	+	-	+	+	-	N. D*	BL	BL
3	65/F	+	≧ 90%	+	+	-	+	-	+	+	-	N. D*	BL	BL
4	73/M	+	≧ 90%	+	+	-	+	-	+	+	-	N. D*	BL	BL
5	16/M	+	≧ 90%	+	+	-	+	+	+	+	-	N. D*	BL	BL
6	20/F	+	≧ 90%	+	+	-	+	-	+	+	-	N. D*	BL	BL
7	82/M	+	≧ 90%	+	+	-	+	-	+	+	-	N. D*	BL	BL
8	54/M	+	≧ 90%	+	+	-	+	-	+	+	-	N. D*	BL	BL
9	40/F	+	≧ 90%	+	+	-	+	-	+	+	-	N. D*	BL	BL
10	39/F	-	≧ 90%	+	+	-	-	-	+	+	-	complex**	BLL	iDLBCL/BL
11	42/M	+	≧ 90%	+	+	+	-	-	+	+	-	N. D*	BL	iDLBCL/BL

The results of the morphological, immunophenotypical, and genetical analysis of the patients were shown. All patients were re-diagnosed according to the v4 classification. N.D.; not determined

complex**; 50 XX, +3, add (6) (q21), del (6) (q?), +7, add (14) (q32), add (17) (q11,2)+18, +mar1

Table 3. Laboratory data at diagnosis

Case No.	Age/Sex	WBC (/μL)	Hgb (g/dL)	Plt (x 10^4/μL)	LDH (U/L)	CRP (mg/dL)	sIL-2R (U/mL)
1	46/F	4,300	14.1	25.8	299	1.04	571
2	70/M	8,110	13.9	21.4	396	3.42	692
3	65/F	5,400	11.2	29.2	203	0.78	490
4	73/M	4,900	15.9	16.5	929	0.25	753
5	16/M	7,600	17.5	35.0	374	0.08	983
6	20/F	27,900	12.2	58.7	751	29.33	11,826
7	82/M	5,700	14.0	25.4	149	0.01	279
8	54/M	7,400	11.3	24.2	564	2.52	4,560
9	40/F	6,500	9.4	46.0	312	0.47	580
10	39/F*	25,000	9.5	7.9	1,204	9.59	31,328
11	42/M*	4,500	12.3	32.1	1,004	4.03	1,596

WBC; white blood cell count, Hgb; hemoglobin level, Plt; platelet count, LDH; lactate dehydrogenase, CRP; C-reactive protein, sIL-2R; soluble interleukin-2 receptor, *; Patients with iDLBCL/BL

with 3 patients aged > 70 years. Nine out of 11 patients were in advanced stages (stage III or IV) at the diagnosis. Eight patients exhibited extranodal involvement (Table 1).

When all 11 cases were re-evaluated according to the v4 WHO classification (Table 2), 9 of the 10 cases originally diagnosed as BL showed typical "starry sky" morphology, positive staining for CD20 and BCL6, negative staining for BCL2, > 90% positive for Ki-67 staining, and *cMYC* rearrangement upon FISH analysis. Thus, the diagnosis of BL was unchanged for these cases.

The diagnosis of one (UNP11) of the ten cases whose original diagnosis was BL was changed to iDLBCL/BL because of strongly positive BCL2 staining, despite the fact that all other features were compatible with BL. None of the cases including UNP11 demonstrated *BCL2* rearrangement. The one case originally diagnosed as BLL (UNP10) was re-diagnosed as iDLBCL/BL because of the presence of large B cells that were recognizable as tumor cells, which matched the morphological criteria of iDLBCL/BL.

G-banding analysis in one iDLBCL/BL case (UNP10) showed a complex karyotype, while cytogenetic data were not available in other patients (Table 1).

LDH and sIL-2R levels were elevated in 7 BL patients. Two iDLBCL/BL patients had extranodal involvement with high LDH and sIL2-R levels (Tables 1 & 3).

Response to therapy and outcome

Of the 11 patients, "prephase" treatment was given to 10 patients (8 BL and 2 iDLBCL/BL) because they had bulky mass, as well as 7 patients (5 BL and 2 iDLBCL/BL) with a poor general condition (Table 1). As the prephase treatment, 5 patients (4 BL and 1 iDLBCL/BL) were given a COP or a CHOP regimen while the remaining 5 patients were given PSL alone.

After the two courses of induction regimen, 10 patients (9 BL and 1 iDLBCL/BL) achieved CR or CRu. All the 9 BL patients maintained progression-free survival for 38-118

months (median 56 months, Table 1). For reasons of old age (UNP 7) and poor general condition (UNP 2), the consolidation regimens were omitted in one case (UNP 7) and both the second induction regimen and the two consolidation regimens were omitted in another case (UNP 2); instead, radiation therapy for the residual lesion was provided. Both patients have shown no signs of relapse and are still alive 3 and 9 years later, respectively.

Both iDLBCL/BL patients died from infection after the first induction therapy and CNS relapse.

Toxicity of treatment

Myelosuppression was the main form of toxicity. Febrile neutropenia was observed in 7 (63%) patients after first induction regimen. Grade III/IV thrombocytopenia and anemia were observed in 4 (36%) and 2 (18%) patients, respectively (Table 4). Two patients suffered from acute renal dysfunction but recovered without recourse to hemodialysis. Tumor lysis syndrome during and after the first induction regimen was experienced in one iDLBCL/BL patient (UNP 10), who died from peritonitis and sepsis compromised by tumor lysis syndrome despite the prephase (CHOP) therapy.

The incidence of therapy-related toxicity was much lower in the second course of induction regimen than in the first course (grade III/IV thrombocytopenia, 36% *vs.* 10%; febrile neutropenia, 63% *vs.* 30% in the first and second courses, respectively; Table 4). However, grade III/IV hematologic toxicities and febrile neutropenia were frequently observed after consolidation #1 (anemia, 77%; thrombocytopenia, 87.5%; febrile neutropenia, 77%). Although grade III mucositis was documented in 36, 20, and 37% after the treatment, which included HD-MTX (first induction, second induction, and consolidation #2, respectively), the median period required for the recovery to the grade II level or less was 5 days. No grade IV mucositis was documented.

There were no obvious additional toxicities in patients who received rituximab.

DISCUSSION

Intensive chemotherapy regimens that include HD-MTX as well as high-dose AraC and CPA[13] were developed for pediatric BL and later applied to adult BL. This development appears to have improved the prognosis of adult BL.[3-5,8,10,14,15] The effectiveness of LMB protocol for adult BL was reported in 1995,[10] which was one of the earliest reports describing successful treatment of adult BL using HD-MTX. The original CODOX-M/IVAC was also reported by Magrath *et al.* in 1996,[3] although this protocol was modified through clinical studies;[4,5] the reduction of MTX was among major changes because the principal cause of toxicity in the original CODOX-M/IVAC was the use of MTX at 6.7 g/m^2 in a single course. While there is a consensus on the necessity of HD-MTX for BL treatment, the MTX dose and timing are under debate.

Most of the ensuing confirmatory studies, however, in addition to the original LMB and CODOX-M/IVAC studies, were performed with European and North American populations, while a retrospective analysis using LMB protocol for adult BL was previously reported from a Korean group.[7] This raises the question of whether the same results can be produced in Japanese populations. For this reason, we retrospectively analyzed whether a modified LMB protocol in adult Japanese BL patients would be efficient and feasible.

For the 9 patients < 70 years, MTX was given at 5 g/m^2 in the first and second courses of the induction regimen and at 3 g/m^2 in the consolidation #2 regimen, meaning that 13 g/m^2 was delivered in total over 4 courses of chemotherapy. The toxicities during the induction phase were well tolerated, with close monitoring of MTX level in the serum. All the 6 BL patients who received the modified LMB protocol as planned have survived for more than 3 years, which indicates that intensive chemotherapy including MTX at high doses such as 13 g/m^2 in total is both tolerable and effective for Japanese BL patients < 70 years. The LMB-like protocol may be suitable to treat Asian BL patients, as was suggested by a

Table 4. Frequency of adverse events during the treatment

Toxicity (%)	Induction 1	Induction 2	Consolidation 1	Consolidation 2
Anemia	18	0	75	11
Thrombocytopenia	36	10	87	0
Febrile neutropenia	63	30	77	11
Mucositis	36*	20	0	37*
Neuropathy	9*	0	0	0
Bilirubin	18*	0	0	0
Renal failure	18	0	0	0
Tumor lysis syndrome	18*	0	0	0

Grade III/IV toxicities and adverse events related to chemotherapy are shown. Toxicities and adverse events related to chemotherapy were assessed and graded according to the National Cancer Institute Common Toxicity Criteria, version 2.0.
*; No Grade IV toxicity was documented.

previous report from Korea.[7] Our results also suggest that BL could be curable with less intensive chemo-radiotherapy, given that all the 3 elderly patients who received a reduced dose have survived for more than 3 years.

In conclusion, not only the modified CODOX-M/IVAC protocol[16] but also the modified LMB protocol is effective and tolerable in Japanese adult BL patients *aged* < 70. For elderly patients, reduced dose and/or cycles of chemotherapy may be required, and reduced doses could be effective.

Declaration of interest : The authors report no conflicts of interest. The authors are responsible for the content and writing of the paper.

REFERENCES

1 Perkins AS, Friedberg JW: Burkitt lymphoma in adults. Hematology Am Soc Hematol Educ Program 341-348, 2008

2 Blum KA, Lozanski G, Byrd JC: Adult Burkitt leukemia and lymphoma. Blood 104:3009-3020, 2004

3 Magrath I, Adde M, Shad A, Venzon D, Seibel N, *et al.*: Adults and children with small non-cleaved-cell lymphoma have a similar excellent outcome when treated with the same chemotherapy regimen. J Clin Oncol 14:925-934, 1996

4 Mead GM, Sydes MR, Walewski J, Grigg A, Hatton CS, *et al.*: An international evaluation of CODOX-M and CODOX-M alternating with IVAC in adult Burkitt's lymphoma: results of United Kingdom Lymphoma Group LY06 study. Ann Oncol 13:1264-1274, 2002

5 Mead GM, Barrans SL, Qian W, Walewski J, Radford JA, *et al.*: A prospective clinicopathologic study of dose-modified CODOX-M/IVAC in patients with sporadic Burkitt lymphoma defined using cytogenetic and immunophenotypic criteria (MRC/NCRI LY10 trial). Blood 112:2248-2260, 2008

6 Barrans SL, Evans PA, O'Connor SJ, Owen RG, Morgan GJ, *et al.*: The detection of t (14;18) in archival lymph nodes: development of a fluorescence in situ hybridization (FISH)-based method and evaluation by comparison with polymerase chain reaction. J Mol Diagn 5:168-175, 2003

7 Choi MK, Jun HJ, Lee SY, Kim KH, Lim do H, *et al.*: Treatment outcome of adult patients with Burkitt lymphoma: results using the LMB protocol in Korea. Ann Hematol 88:1099-1106, 2009

8 Divine M, Casassus P, Koscielny S, Bosq J, Sebban C, *et al.*: Burkitt lymphoma in adults: a prospective study of 72 patients treated with an adapted pediatric LMB protocol. Ann Oncol 16:1928-1935, 2005

9 Galicier L, Fieschi C, Borie R, Meignin V, Daniel MT, *et al.*: Intensive chemotherapy regimen (LMB86) for St Jude stage IV AIDS-related Burkitt lymphoma/leukemia: a prospective study. Blood 110:2846-2854, 2007

10 Soussain C, Patte C, Ostronoff M, Delmer A, Rigal-Huguet F, *et al.*: Small noncleaved cell lymphoma and leukemia in adults. A retrospective study of 65 adults treated with the LMB pediatric protocols. Blood 85:664-674, 1995

11 Cheson BD, Horning SJ, Coiffier B, Shipp MA, Fisher RI, *et al.*: Report of an international workshop to standardize response criteria for non-Hodgkin's lymphomas. NCI Sponsored International Working Group. J Clin Oncol 17:1244, 1999

12 Trotti A, Byhardt R, Stetz J, Gwede C, Corn B, *et al.*: Common toxicity criteria: version 2.0. an improved reference for grading the acute effects of cancer treatment: impact on radiotherapy. Int J Radiat Oncol Biol Phys 47:13-47, 2000

13 Kujawski LA, Longo WL, Williams EC, Turman NJ, Brandt N, *et al.*: A 5-drug regimen maximizing the dose of cyclophosphamide is effective therapy for adult Burkitt or Burkitt-like lymphomas. Cancer Invest 25:87-93, 2007

14 Lee EJ, Petroni GR, Schiffer CA, Freter CE, Johnson JL, *et al.*: Brief-duration high-intensity chemotherapy for patients with small noncleaved-cell lymphoma or FAB L3 acute lymphocytic leukemia: results of cancer and leukemia group B study 9251. J Clin Oncol 19:4014-4022, 2001

15 Thomas DA, Faderl S, O'Brien S, Bueso-Ramos C, Cortes J, *et al.*: Chemoimmunotherapy with hyper-CVAD plus rituximab for the treatment of adult Burkitt and Burkitt-type lymphoma or acute lymphoblastic leukemia. Cancer 106:1569-1580, 2006

16 Maruyama D, Watanabe T, Maeshima AM, Nomoto J, Taniguchi H, *et al.*: Modified cyclophosphamide, vincristine, doxorubicin, and methotrexate (CODOX-M)/ifosfamide, etoposide, and cytarabine (IVAC) therapy with or without rituximab in Japanese adult patients with Burkitt lymphoma (BL) and B cell lymphoma, unclassifiable, with features intermediate between diffuse large B cell lymphoma and BL. Int J Hematol 92:732-743, 2010

Brief report

Successful sustained engraftment after reduced-intensity umbilical cord blood transplantation for adult patients with severe aplastic anemia

Hisashi Yamamoto,[1] Daisuke Kato,[1] Naoyuki Uchida,[1] Kazuya Ishiwata,[1] Hideki Araoka,[2] Shinsuke Takagi,[1] Nobuaki Nakano,[1] Masanori Tsuji,[1] Yuki Asano-Mori,[1] Naofumi Matsuno,[1] Kazuhiro Masuoka,[1] Koji Izutsu,[1] Atsushi Wake,[1] Akiko Yoneyama,[2] Shigeyoshi Makino,[3] and Shuichi Taniguchi[1,4]

Departments of [1]Hematology, [2]Infectious Diseases, and [3]Transfusion Medicine, Toranomon Hospital, Tokyo, Japan; and [4]Okinaka Memorial Institute for Medical Research, Tokyo, Japan

We retrospectively analyzed 12 consecutive adult severe aplastic anemia patients who received unrelated umbilical cord blood transplantation after a reduced-intensity conditioning regimen (RI-UCBT). The conditioning regimen consisted of 125 mg/m^2 fludarabine, 80 mg/m^2 melphalan, and 4 Gy of total body irradiation. The median infused total nucleated cell number and CD34$^+$ cell number were 2.50 × 10^7/kg and 0.76 × 10^5/kg, respectively. Eleven of the 12 patients achieved primary neutrophil and platelet engraftment. All patients who achieved engraftment had complete hematologic recovery with complete donor chimerism, except for one patient who developed late graft failure 3 years after RI-UCBT. Two of the 12 patients died of idiopathic pneumonia syndrome, and the remaining 10 patients are alive, having survived for a median of 36 months. Our encouraging results indicate that RI-UCBT may become a viable therapeutic option for adult severe aplastic anemia patients who lack suitable human leukocyte antigen-matched donors and fail immunosuppressive therapy. (*Blood*. 2011;117(11):3240-3242)

Introduction

Bone marrow transplantation from a human leukocyte antigen (HLA)-matched sibling is recommended as first-line therapy for younger patients with severe aplastic anemia (SAA).[1,2] However, many patients lack HLA-matched sibling donors. Bone marrow transplantation from an HLA-matched unrelated donor has been an alternative therapeutic option for patients who fail one or more courses of immunosuppressive therapy, but high rates of graft failure (GF), graft-versus-host disease (GVHD), and infection still remain to be solved.[3] The number of unrelated umbilical cord blood transplantations (UCBTs) has been increasing.[4] However, little information has been available on whether UCBT is feasible for SAA patients. We reported successful urgent UCBT using reduced-intensity (RI) conditioning for a 70-year-old SAA patient in 2003.[5] Here we present successful sustained engraftment of 11 consecutive patients with SAA who received RI-UCBT with the same RI conditioning regimen after the first report.

Methods

This study included 12 consecutive adult patients with acquired SAA who underwent RI-UCBT at our institute from September 2002 through January 2009. The patients' characteristics and umbilical cord blood (UCB) units are summarized in Table 1. Their median age was 49 years (range, 20-70 years). Four cases of severe, 6 of very severe, and 2 of fulminant type were included according to criteria as previously reported.[2,6] Fulminant type was defined as no neutrophils in the peripheral blood at diagnosis despite administration of granulocyte-colony stimulating factor. Ten patients, except for the 2 patients with fulminant type, had failed at least one course of immunosuppressive therapy. All patients gave their written informed consent in accordance with the Declaration of Helsinki, and the study was approved by the Toramon Hospital Institutional Review Board. UCB units were obtained from the Japanese Cord Blood Bank Network, and single UCB unit was infused in all the studied patients. All UCB units were serologically typed for HLA-A, -B, and -DR antigen before selection and were tested by high-resolution DNA typing before transplantation. The degree of mismatch is expressed using antigen level at HLA-A and -B, and allele level at DRB1. ABO incompatibility was not incorporated as one of the factors used in CB unit selection. The median total nucleated cell number and CD34$^+$ cell number at cryopreservation were 2.50 × 10^7/kg (range, 1.83-4.39 × 10^7/kg) and 0.76 × 10^5/kg (range, 0.27-1.52 × 10^5/kg), respectively. Anti-HLA antibodies were screened before transplantation in 6 patients using a FlowPRA method (One Lambda), and LAB Screen PRA or Single Antigen (One Lambda) was used to identify HLA antibody specificities.[7,8] All patients were conditioned with 25 mg/m^2 fludarabine daily for 5 days, 40 mg/m^2 melphalan daily for 2 days, and 4 Gy of total body irradiation in 2 fractions in 1 day. GVHD prophylaxis consisted of cyclosporine in 2, tacrolimus in 2, and tacrolimus plus mycophenolate mofetil in 8. Assessment of engraftment, GF, chimerism, GVHD, and supportive care during transplantation were performed as previously reported.[9,10] Karnofsky performance status score was assessed as surrogate for quality of life of the survivors. Overall survival was estimated using the Kaplan-Meier method.

Results and discussion

Patients' outcomes are summarized in Table 2. Eleven of the 12 patients achieved primary neutrophil and platelet engraftment. The median times to achieve neutrophil engraftment and platelet count more than 20 × 10^9/L were 18 days (range, 12-28 days) and

Submitted August 21, 2010; accepted December 25, 2010. Prepublished online as *Blood* First Edition paper, January 13, 2011; DOI 10.1182/blood-2010-08-295832.

The publication costs of this article were defrayed in part by page charge payment. Therefore, and solely to indicate this fact, this article is hereby marked "advertisement" in accordance with 18 USC section 1734.